NATIONAL INSTITUTE OF POLAR RESEARCH

ANTARCTIC GEOLOGICAL MAP SERIES
SHEET 38 TONAGH ISLAND

Explanatory Text of Geological Map
of
Tonagh Island, Enderby Land, Antarctica

Yasuhito OSANAI, Tsuyoshi TOYOSHIMA, Masaaki OWADA, Toshiaki TSUNOGAE
Tomokazu HOKADA, Yasutaka YOSHIMURA, Tomoharu MIYAMOTO,
Yoichi MOTOYOSHI, Warwick A. CROWE, Simon L. HARLEY,
Masaki KANAO and Masao IWATA

NATIONAL INSTITUTE OF POLAR RESEARCH
TOKYO, MARCH 2001

9–10, Kaga 1-chome, Itabashi-ku, Tokyo 173-8515

Antarctic Geological Map Series
Sheet 38

Tonagh Island

Explanatory Text of Geological Map of Tonagh Island, Enderby Land, Antarctica

Yasuhito Osanai [1], Tsuyoshi Toyoshima [2], Masaaki Owada [3], Toshiaki Tsunogae [4], Tomokazu Hokada [5], Yasutaka Yoshimura [6], Tomoharu Miyamoto [7], Yoichi Motoyoshi [5], Warwick A. Crowe [8], Simon L. Harley [9], Masaki Kanao [5] and Masao Iwata [10]

NATIONAL INSTITUTE OF POLAR RESEARCH, TOKYO, MARCH 2001

[1] Department of Earth Sciences, Faculty of Education, Okayama University, Okayama 700-8530
[2] Department of Geology, Graduate School of Science and Technology, Niigata University, Niigata 950-2181
[3] Department of Earth Sciences, Faculty of Science, Yamaguchi University, Yamaguchi 753-8512
[4] Department of Earth Sciences, Faculty of Education, Shimane University, Matsue 690-8504
[5] National Institute of Polar Research, Tokyo 173-8515
[6] Department of Natural Environmental Sciences, Faculty of Science, Kochi University, Kochi 780-8520
[7] Department of Earth and Planetary Sciences, Faculty of Sciences, Kyushu University, Fukuoka 812-8581
[8] Department of Geology and Geophysics, Faculty of Science, University of Western Australia, Perth 6907, Australia
[9] Department of Geology and Geophysics, University of Edinburgh, Edinburgh EH9 3JW, Scotland, United Kingdom
[10] Geograhical Survey of Institute of Japan, Tsukuba 305-0821

Contents

1. Introduction

Tonagh Island (67°05'51"S, 50°17'19"E) is one of the largest isolated islands and is located in the southern-end of Amundsen Bay, Enderby Land, East Antarctica (Fig. 1). Geological survey of the Enderby Land established at Proclamation Island in 1930 operated by British, Australian and New Zealand Antarctic Research Expedition (BANZARE) led by Douglas Mawson (Mawson, 1932). During the two decades of 1950s and 1960s, geologists from Australian Bureau of Mineral Resources made brief studies to scattered localities throughout Enderby Land attached to the Australian National Antarctic Research Expedition (ANARE) (e.g. Crohn, 1959; McLeod, 1959, 1964; Rucker, 1963; McLeod *et al.*, 1966). Geologists of the Soviet Antarctic Expedition (SAE) carried out more extensive 1:1,000,000-scale geological mapping of Enderby Land during the 1960s (e.g. Kamenev, 1972, 1975; Grikurov *et al.*, 1976). Then the SAE geologists distinguished two metamorphic complexes of the Napier Complex and the Rayner Complex basically owing to their metamorphic grade and age differences (Grikurov *et al.*, 1976). The ANARE geologists performed helicopter-supported systematic regional geological survey throughout the Enderby Land in 1974 – 1980 with making a brief geological map covering whole outcrops of the Napier Complex, Enderby Land (Sheraton, 1985; Sheraton *et al.*, 1987).

The Japanese Antarctic Research Expedition (JARE) also has been conducted short term but continuous geological surveys and investigations around the Amundsen Bay and Casey Bay areas of Enderby Land during these two decades. Mount Riiser-Larsen area (66°45'S, 50°45'E), which is located on the northern coastline of Adams fjord along Amundsen Bay, was visited by many JARE geologists as JARE-23, -29,

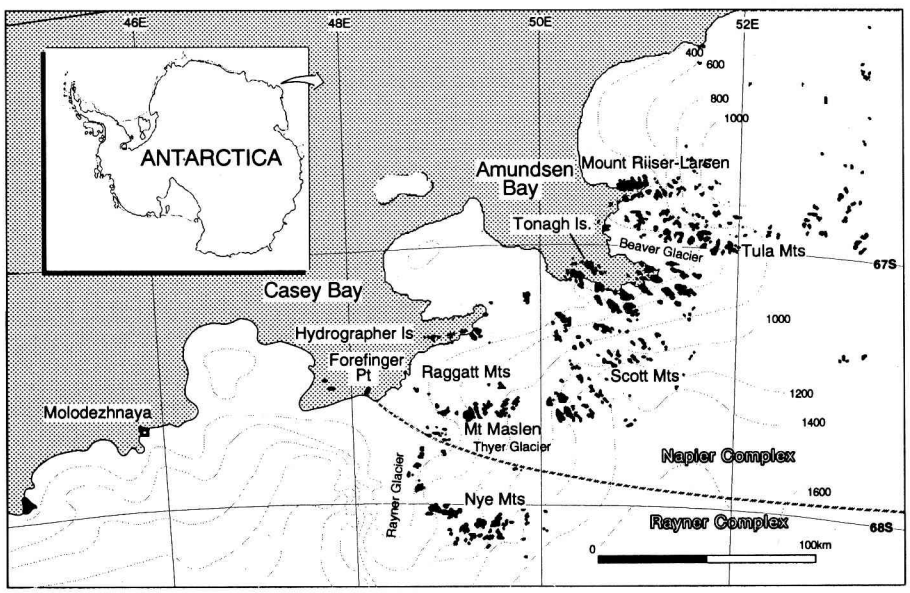

Fig. 1 Location map of Tonagh Island. The boundary between the Napier Complex and the Rayner Complex is after Sheraton et al. (1987).

-34, -36, -37, -38, -39 and -40. Tonagh Island and Mount Pardoe have also been visited several times by JARE-31, -39 and –40. Recently JARE geologists are expanding their survey area i.e., McIntyre and Hydrographer Islands, Mount Maslen, and Forefinger Point by JARE-34, Bunt Island and Priestley Peak by JARE-39, and Howard Hills, Field Island and Edwards Island by JARE-40.

The geological outline for the whole region of the Napier Complex was reported by Sheraton (1985) for the geological map and Sheraton *et al.* (1987) for explanatory text. After this, detailed geological investigations including geological mapping has only been done a few times (e.g. East Tonagh Island by Harley, 1987 and a part of Mount Riiser-Larsen by Makimoto *et al.*, 1989). In 1996, the Japanese Antarctic Research Expedition (JARE) established a new earth scientific project "SEAL" (Structure and Evolution of east Antarctic Lithosphere). This project includes two types of geological research program: (1) regional geological investigation throughout the Napier and the Rayner Complexes and (2) local but detailed geological investigation in a specific area. During the first austral summer season (1996-1997), a JARE-38 party carried out a detailed geological survey at Mount Riiser-Larsen with making a geological map (Ishizuka *et al.*, 1998; Ishikawa *et al.*, 2000). Then in the second season a JARE-39 party did a careful geological survey on Tonagh Island to make a detailed geological map from January 24, 1998 to February 22, 1998 (Osanai *et al.*, 1999). During 1998-1999 Antarctic summer season, a JARE-40 geology team also performed a supplementary geological fieldwork in Tonagh Island (Motoyoshi *et al.*, 1999).

This edition of the Antarctic Geological Map Series, Sheet 38 "Tonagh Island" incorporate the field data and laboratory work by JARE-39 and JARE-40 for Tonagh Main Island and the Simon Harley's lead data for East Tonagh Island (Harley, 1987).

2. General Geology

Tonagh Islands are located at the southern end of Amundsen Bay between the Tula Mountains and the Scott Mountains, Enderby Land, which belongs to the central Napier Complex (Fig. 1). The islands are part of the highest-grade metamorphic region in the Napier Complex (Grew, 1982; Harley and Hensen, 1990) (Fig. 2). Tonagh Islands actually consist of three islands: East Tonagh Island (3 x 2 km), Tonagh Main Island (hereafter Tonagh Island: 5 x 6 km), and West Tonagh Island (2 x 1 km). West Tonagh Island is completely covered by Cenozoic deposit (glacial till?). On the other hand, detailed studies of metamorphism for meta-iron stone and pyroxene granulites from East Tonagh Island including geological mapping of the whole island have been carried out by Harley (1987). Therefore, JARE geology teams carried out the geological survey on Tonagh Island. Tonagh Island is geomorphologically divided into three major parts, nearly flat terrace in the southern, northeastern and western areas, plateau peninsular in the northern area, and steep mountain ridges extending NW-SE in the central area. The central mountain ridge shows a steep slope or cliff along the western, southern and eastern sides, while the northern slope is gentle down to the northeastern terrace and partly covered by thick Cenozoic deposit of till- or talus-type. The highest peak of Tonagh Island is c. 480 m above sea level (Plate 1).

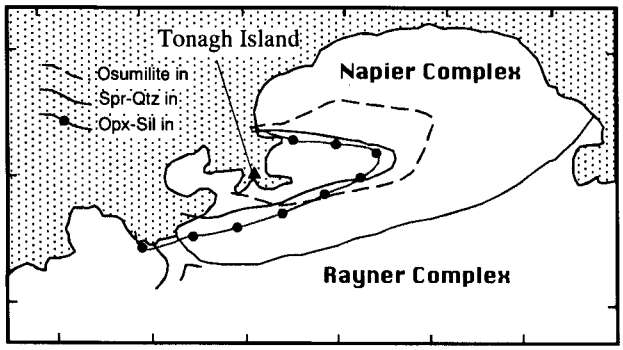

Fig. 2 High-grade region of the Napier Complex which is characterized by the isograds of 'osumilite in', 'sapphirine-quartz (Spr-Qtz) in' and 'spinel-quartz (Spl-Qtz) in', after Harley and Hensen (1990).

Archaean to early Proterozoic regional ultrahigh-temperature (UHT) metamorphic rocks are widely exposed in the Napier Complex, northern Enderby Land (e.g. Sheraton *et al.*, 1987). The dominant rock types of the Napier Complex are pyroxene- and garnet-bearing quartzo-feldspathic gneisses of igneous origin (Archaean TTG-type tonalitic orthogneiss); subordinate constituents are considered to be ultramafic, mafic, pelitic, and siliceous granulites. Some of these gneisses and granulites have been characterized by UHT-type mineral assemblages of spinel+quartz and garnet+sapphirine+quartz, with or without orthopyroxene and osumilite, and orthopyroxene+sillimanite+quartz (e.g. Dallwitz, 1968; Sheraton *et al.*, 1980; Ellis, 1980; Grew, 1980; Harley, 1985, 1998; Sandiford, 1985; Motoyoshi and Matsueda, 1984; Motoyoshi and Hensen, 1989; Motoyoshi *et al.*, 1990, 1994, 1995; Hokada *et al.*, 1999; Tsunogae *et al.* 1999). Characteristic high-fluorine biotite is also present as a primary phase (Osanai *et al.*, 1995; Motoyoshi, 1998). The P-T conditions of these granulites are up to 800-1000 MPa and 1000-1100°C, found by Harley and Hensen (1990), Harley (1998), Hokada *et al.* (1999) and Yoshimura *et al.* (2000). The age of these rocks had been determined by ion microprobe U-Pb analyses, and Sm-Nd and Rb-Sr whole rock isochron methods. The results indicate that the tonalitic precursor of the orthogneiss had intruded into the crust at c.3950-3700 Ma (Williams *et al.*, 1984; Black *et al.*, 1986a; Owada *et al.*, 1994; Harley and Black, 1997) and then the main metamorphism in the complex occurred at c. 2800 Ma (Harley and Black, 1997) or c.2500 Ma (e.g. Grew and Manton, 1979; DePaolo *et al.*, 1982; Black *et al.*, 1986b; Owada *et al.*, 1994; Tainosho *et al.*, 1994; Shiraishi *et al.*, 1997; Asami *et al.*, 1998). Geological structure (Griffin, 1979; James and Black, 1981; Sandiford and Wilson, 1983, 1984; Harley, 1987; Ishikawa *et al.*, 1994; Toyoshima *et al.*, 1999), geochemistry (Sheraton, 1980, 1984; Sheraton and Black, 1981, 1983; Sheraton *et al.*, 1987; Tainosho *et al.*, 1994, 1997; Owada *et al.*, 1994, 1999, 2000; Suzuki *et al.*, 1999) and geophysics (Wellman, 1983; Wellman and Tingey, 1982) are also investigated in detail.

Tonagh and East Tonagh Islands are underlain by various kinds of metamorphic rocks and subordinate amounts of three types of unmetamorphosed intrusive rocks (dolerite, lamproite and granitic pegmatite). Metamorphic rocks from Tonagh Island are subdivided into five lithologic units (Units I to V) owing to their lithologies and structures from north to south. Geology of Units I, II and III are characterized by modes

of occurrence of thick mafic granulites and layered gneiss sequences. However, Units IV and V of Tonagh Island and East Tonagh Island are characteristically free from thick mafic granulite and layered gneiss sequence. The boundaries of each unit are NE-SW to E-W trending steeply north, dipped or near vertical thrusts or shear zones accompanying with remarkable anhydrous mylonite and later pseudotachylite-cataclasite. These thrusts or shear zones cut across the island with width of several to hundreds of meters. The distinctive metamorphosed mafic dikes of tholeiitic composition are also found along the shear zone, characteristically at the boundary between Units II and III and East Tonagh Island. Metamorphic foliations in each unit are different from each other. The Unit I metamorphic foliation strikes NE-SW and dips at a steep angle (50-80°) to the SE or NW, forming small-scale synforms and antiforms. Those in Units II and III show nearly the same strikes (partly N-S direction only at the eastern part of Unit III) but gentler dips (15-40°) to the NW except along the sheared unit-boundaries, where metamorphic foliations bend with rather steep dips (50-60°). In Units IV and V, metamorphic foliations strike NE-SW to E-W and dip to the north with moderate angle (20-60°). There are some multi-stage-deformed synforms and antiforms especially in Unit II, Unit V and East Tonagh Island, with local variation of metamorphic foliations. The preferred orientation of metamorphic minerals as well as mineral lineation is generally quite weak or invisible. The unmetamorphosed dolerite dikes, which are designated the Amundsen Dykes (e.g. Sheraton *et al.*, 1987), cut across not only the sequence of metamorphic rocks but also the unit boundary shear zone and metamorphosed mafic dike.

A geological perspective of the metamorphic rocks from Tonagh Islands is generally classified into nine types on the regional map scale as follows:

1) layered gneiss 1 (composed mainly of mafic gneiss and orthopyroxene-bearing quartzo-feldspathic gneiss with subordinate various gneisses and granulites),
2) layered gneiss 2 (composed mainly of mafic gneiss and garnet-bearing quartzofeldspathic gneiss with subordinate various gneisses and granulites),
3) orthopyroxene-bearing felsic gneiss,
4) garnet-bearing felsic gneiss,
5) two pyroxene-bearing mafic granulite,
6) garnet-orthopyroxene gneiss and granulite,
7) magnetite-quartz gneiss,
8) ultramafic granulite,
9) garnet-two pyroxene metamorphosed mafic dyke.

As may be seen in geological map the metamorphic rock assembly as well as protolith of the metamorphic rocks of Unit I (northern area), of Units II to IV (central area), and of Unit V (southern area) and East Tonagh Island are clearly different. The orthopyroxene-bearing quartzo-feldspathic charnockitic gneiss and garnet-bearing quartzo-feldspathic gneiss are the main constituents of Tonagh Island. The Unit I has a peculiarity of predominance of layered gneisses showing thin alternation (millimeters to several meters in thickness) of orthopyroxene- and garnet-bearing quartzo-feldspathic gneisses, two pyroxene mafic granulite, garnet-orthopyroxene gneiss and granulite, sapphirine-bearing aluminous gneiss, garnet-sillimanite gneiss, leucocratic quartzo-feldspathic gneiss, magnetite-quartz gneiss, meta-quartzite and metamorphosed ultramafic rocks (pyroxenite and lherzolite). Units II and III are characterized by widespread distributions of two pyroxene-bearing mafic granulite (gneiss) and garnet-orthopyroxene gneiss at the upper

structural level, although layered gneisses dominate at the lower structural level by the homoclinal and downward stratigraphic polarity to the East. In field appearance Unit II and Unit III have nearly the same lithology, this may be considered repetition due to thrusting. The magnetite-quartz gneiss occurs mainly in Units I, II and III, but rare in East Tonagh Island. Unit IV is underlain by garnet- and orthopyroxene-bearing quartzo-feldspathic gneisses and layered gneisses, which looks very close to the lower structural level of Units II and III. On the other hand, constituents of Unit V and East Tonagh Island are mainly orthopyroxene- and garnet-bearing quartzo-feldspathic gneisses with subordinate layered gneiss 1 and traces of aluminous, mafic and ultramafic gneisses. Therefore the most effective tectonic boundary may be the shear zone among Units IV and V. More detailed descriptions of modes of occurrence, with brief petrographical features of each metamorphic rock are given below.

3. Metamorphic Rocks

The rock classification using protoliths is difficult for high- and ultrahigh-temperature metamorphic rocks, so we named the rocks using only modal variations and assemblages of metamorphic minerals. The metamorphic rocks are classified into nine rock types including the six types (3 to 9) mentioned above, but excepting two types of layered gneisses, and adding three other types as follows: 10) sapphirine-bearing aluminous gneiss, 11) metamorphosed impure quartzite and 12) calc-silicate granulite. In this chapter we describe the modes of occurrence with brief description of petrographical features of each metamorphic rock. Two types of layered gneisses and the first seven rock types mentioned above are relatively major lithologic facies, which are illustrated on the regional scale geological map. The latter three types are minor and occur only as thin intercalations or blocks in layered gneisses 1 and 2.

3.1. Layered gneiss 1 (Gl1)

Layered gneiss 1 (Plate 2A) is distributed in Units I, II, III and IV in the Tonagh Island. The layered gneiss 1 is composed mainly of orthopyroxene-bearing felsic gneiss and two pyroxene-bearing mafic granulite with subordinate amounts of many kinds of gneisses and granulites and is showing thin alternation of millimeter to several tens of meter scale. Especially in the eastern part of Unit I the layered gneiss 1 is complicated and includes many thin layers of magnetite-quartz gneiss and impure quartzite. Metamorphosed ultramafic rocks also occur as boudinaged block, which surrounded by sapphirine-bearing garnet-orthopyroxene gneiss and granulite.

3.2. Layered gneiss 2 (Gl2)

Layered gneiss 2 is distributed over the whole region of Tonagh Island and in the eastern part of East Tonagh Island. The gneisses in Units II and III and in East Tonagh Island are observed at the basal part (lower structural level) owing to their regional geological structure. The layered gneiss 2 is more complicated rather than layered gneiss 1 and composed mainly of garnet-bearing felsic gneiss, orthopyroxene felsic gneiss and two pyroxene-bearing mafic granulite with subordinate garnet-

orthopyroxene gneiss (relatively leucocratic) and granulite (melanocratic), garnet-sillimanite gneiss, sapphirine-bearing aluminous gneiss, sapphirine-bearing impure quartzite, metamorphosed ultramafic rocks *etc.* Especially, layered structure of the Layered gneiss 2 is dominated in the northern peninsular area (Plate 2B). Details of each rock in layered gneisses 1 and 2 are described below.

3.3. Orthopyroxene-bearing felsic gneiss (Gof)

Orthopyroxene-bearing felsic gneiss (felsic orthopyroxene gneiss, which is equivalent to the gneiss described by Ishizuka *et al.*, 1998 and Ishikawa *et al.*, 2000) is widespread in the whole area of Tonagh Island as not only thick layers (up to 400 m in thickness) but also thin intercalations (centimeter to meter in scale) among the layered gneisses (Plate 2C). The felsic orthopyroxene gneiss is commonly homogeneous, but well foliated. Compositional layering accompanying modal variations in mineral compositions in felsic orthopyroxene gneiss can also be observed. The felsic orthopyroxene gneiss is normally pale grayish brown to pale brown in color and medium in grain size. Part of the gneiss shows charnockitic pale greenish color. Very fine grained pale greenish schistose felsic orthopyroxene gneiss (mylonite - ultramylonite) without any hydrous minerals is locally developed along the small-scale shear band obliquely cutting the general foliation of felsic orthopyroxene gneiss.

The felsic orthopyroxene gneiss generally shows granoblastic texture with pleochroic orthopyroxene, K-feldspar, plagioclase and quartz as major constituents (Plate 5A). The first three minerals usually have euhedral to subhedral crystal shape, while quartz is normally anhedral. Modal variations of K-feldspar and plagioclase are wide. orthopyroxene is sometimes replaced by green hornblende, biotite and biotite+quartz symplectite along cleavages and/or margins. K-feldspar is mesoperthite to perthite (mainly string- and lod-type). Garnet and clinopyroxene are rarely observed as minor constituents. In particular garnet normally includes plenty of quartz. Accessory minerals are apatite, zircon, ilmenite, magnetite and rutile. The following mineral associations are recognized in the felsic orthopyroxene gneiss:

1) orthopyroxene + biotite + mesoperthite or perthite + plagioclase + quartz,
2) orthopyroxene + mesoperthite or perthite + plagioclase + quartz,
3) orthopyroxene + garnet + mesoperthite or perthite + plagioclase + quartz,
4) orthopyroxene + clinopyroxene + K-feldspar + plagioclase + quartz,
5) orthopyroxene + clinopyroxene + K-feldspar + plagioclase.

Characteristically fine grained mylonitic felsic orthopyroxene gneiss has assemblages 2) or 3) with porphyroclastic orthopyroxene and garnet.

3.4. Garnet-bearing felsic gneiss (Ggf)

Garnet-bearing felsic gneiss is also widespread on Tonagh Island (Plate 2D), especially in the southern part (Units IV and V), several tens to hundreds of meters in thickness. In the northern part (Units I, II and III) several thin layers, ranging in thickness from a few centimeters to meters (up to 80 m), of garnet-bearing felsic gneiss are observed within layered gneisses as intercalations with felsic orthopyroxene gneiss, mafic granulite, magnetite-quartz gneiss and garnet-orthopyroxene gneiss, *etc.* The modal variation of garnet and quartz is highly variable so that the gneiss can be divided into three types: feldspars and quartz dominant garnet-bearing type (pale brown to orange

garnet-bearing quartzofeldspathic gneiss), quartz-rich and garnet-poor type (pale gray to white quartzose garnet gneiss) and garnet predominant type (pale brown to pinkish felsic garnet gneiss). These minute types are not shown on the geological map.

These gneisses normally show granoblastic texture with medium to coarse grained minerals. A well foliated mylonitic part contains porphyroclastic garnet and feldspars and fine elongated quartz and biotite with asymmetrical right-lateral strike-slip sense. The constituent minerals are mainly garnet, plagioclase, K-feldspar including perthite and mesoperthite (Plate 5B), and quartz with or without subordinate amounts of sillimanite, cordierite, spinel, sapphirine, orthopyroxene and biotite. Accessory minerals are rutile, ilmenite, zircon and apatite. The following mineral assemblages are observed in the garnet -baring quartzofeldspathic gneiss, quartzose garnet gneiss and felsic garnet gneiss.

1) garnet + quartz + K-feldspar + plagioclase,
2) garnet + sillimanite + quartz + K-feldspar + plagioclase,
3) garnet + quartz + plagioclase,
4) garnet + sapphirine + sillimanite + cordierite + quartz,
5) garnet + sapphirine + orthopyroxene + sillimanite + quartz,
6) garnet + cordierite + sillimanite + quartz + plagioclase,
7) garnet + sapphirine + orthopyroxene + K-feldspar + plagioclase.

All these assemblages contain biotite as secondary retrograde mineral. Assemblages 1) and 2) are for garnet-bearing quartzofeldspathic gneiss, assemblages 3), 4) and 5) for quartzose garnet gneiss and those of 6) and 7) for felsic garnet gneiss. Green and brown spinels occur as inclusions in sapphirine from assemblage 4) and in garnet from assemblage 5), respectively. In the assemblages 4) and 5), sapphirine and quartz do not show direct contact, but are armored by garnet + cordierite + sillimanite and sillimanite + orthopyroxene+ quartz symplectites, respectively.

3.5. Two pyroxene-bearing mafic granulite (Gm)

Orthopyroxene- and clinopyroxene-bearing mafic granulites occur usually as thick layers (up to 200 m) and also thin intercalations (ranging from several centimeters to meters) in the layered gneisses in Units I, II, III and IV. However, in Unit V, the rocks can be observed in only a few thin layers in layered gneiss 2 excepting one lenticular layer illustrated on the geological map. The boundary between thin layers of two pyroxene-bearing granulite and layers in contact with them among the "layered gneiss" are sometimes oblique and gently cut the metamorphic foliation of neighboring rocks (Plate 2E), which may indicate that the precursor of some two-pyroxene granulite was intrusive rock.

The two pyroxene-bearing mafic granulites are medium- to coarse-grained and granoblastic-polygonal in texture. Normally the granulite is light brownish gray (rather felsic) to light gray (rather mafic) in color. The briefly classified mineral assemblages of the mafic granulites are as follows:

1) orthopyroxene + clinopyroxene + plagioclase + quartz,
2) orthopyroxene + clinopyroxene + pale brown hornblende + plagioclase + quartz,
3) orthopyroxene + clinopyroxene + garnet + plagioclase + quartz,

The assemblages include inverted-pigeonite and subcalsic clinopyroxene. The pyroxenes characteristically include very fine needles of Fe-Ti mineral (mainly ilmenite). Most of

these assemblages also contain secondary hornblende and biotite surrounding pyroxenes (Plate 5C). However at least some biotites, which show high fluorine content, are prograde origin. Rarely, cummingtonite can be found accompanied by greenish hornblende. Part of the garnet, which are rimming pyroxenes, may also be formed during the retrograde stage by the following reactions (1) and (2).

clinopyroxene + plagioclase -> garnet + quartz (1)

orthopyroxene + plagioclase (bytownite) -> garnet + clinopyroxene + quartz + plagioclase (labradorite) (2)

Accessory minerals are apatite, ilmenite and magnetite. Mylonitic two pyroxene-bearing mafic granulite also contains very fine-grained minerals of assemblage 3).

3.6. Garnet-orthopyroxene gneiss and granulite (Ggo)

Garnet-orthopyroxene gneiss and granulite commonly contain garnet and orthopyroxene as major phases. These types of rocks occur generally as thin intercalations ranging from several centimeters to meters in thickness among the layered gneisses, while only in Units II and III relatively thick layers (up to 150 m) occur. Here we name the gneissose and rather felsic portion "garnet-orthopyroxene gneiss", and the massive and rather meranocratic (mafic) portion "garnet-orthopyroxene granulite". Small lenticular blocks and/or pods of garnet-orthopyroxene granulite, which may be of boudinaged origin, are rarely embedded in the orthopyroxene felsic gneiss, garnet felsic gneiss (Plate 2F). In the layered gneisses the garnet-orthopyroxene granulite characteristically crops out at the boundary between ultramafic rock (pyroxenite and lherzolite) and garnet or orthopyroxene-bearing felsic gneisses coexisting with sapphirine-bearing aluminous gneisses (Plate 3A). Garnet-orthopyroxene gneiss is medium-grained pale grayish brown to pale orange, and garnet-orthopyroxene granulite is medium- to coarse-grained dark reddish gray to dark brownish gray in the outcrop. However, both types are commonly related with each other in the outcrop, and one gradually change into another.

The garnet-orthopyroxene granulite comprises mainly garnet, orthopyroxene and plagioclase with occasionally green spinel, sapphirine, cordierite and phlogopite (Plate 5D). Accessories are rutile, ilmenite, magnetite, corundum and apatite. Secondary biotite and gedrite are also present. On the other hand, the garnet-orthopyroxene gneiss consists of garnet, orthopyroxene, quartz with or without feldspars as the major phase, with subordinate brown spinel and clinopyroxene (Plate 5E). Generally, K-feldspar shows rod- and bead-type perthite structures in the garnet-orthopyroxene gneiss. Spinel commonly occurs as inclusions in garnet. Accessories are ilmenite, rutile, apatite and zircon. Secondary biotite is also present. The following assemblages are observed in the garnet-orthopyroxene gneisses (1 - 5) and granulites (6 - 7), except sapphirine-bearing assemblages, which are described in detail at later section 3.9.

1) garnet + orthopyroxene + quartz,
2) garnet + orthopyroxene + quartz + mesoperthite or antiperthite
3) garnet + orthopyroxene + plagioclase + alkali feldspar + quartz,
4) garnet + orthopyroxene + spinel + plagioclase + alkali feldspar + quartz,
5) garnet + orthopyroxene + clinopyroxene + plagioclase + alkali feldspar + quartz,
6) garnet + orthopyroxene + plagioclase,
7) garnet + orthopyroxene + phlogopite + plagioclase.

3.7. Magnetite-quartz gneiss (Gmq)

Magnetite-quartz gneiss, which could be equivalent to the metamorphosed banded iron formation (meta-BIF) on Mount Riiser-Larsen (Ishizuka *et al.*, 1998; Ishikawa *et al.*, 2000) and meta-ironstone in the Napier Complex including East Tonagh Island (Sheraton *et al.*, 1987; Harley, 1987), occurs as thin layers (several centimeters to meters in thickness) in Units I, II and III (Plate 3B). The rock appears black in the magnetite-rich portion and piebald in the quartz- and feldspar-rich portion. Observed mineral assemblages are as follows:

1) magnetite + quartz,
2) magnetite + orthopyroxene + quartz,
3) magnetite + orthopyroxene + clinopyroxene + quartz,
4) magnetite + orthopyroxene + garnet + quartz + plagioclase + K-feldspar.

The rock consists generally of fine- to medium-grained magnetite and quartz matrix with medium- to sometimes coarse-grained orthopyroxene porphyroblast (Plate 5F). Clinopyroxene, garnet, plagioclase, and K-feldspar rarely occur with accessories of apatite and rutile. Orthopyroxene occasionally contains lamella of clinopyroxene as inverted pigeonite which is an indicator of ultrahigh-temperature metamorphism.

3.8. Ultramafic granulite (Gu)

UHT metamorphosed ultramafic rocks are distributed sporadically as thin layers (a few tens of centimeters to meters in thickness) and as boudinaged lenticular or rounded blocks (generally a few tens of meters in diameter) on Tonagh Island (Plate 3C, 3D). These rocks are commonly massive, medium- to coarse-grained, and show three rock types of orthopyroxenite (pale green to pale brown), clinopyroxenite (black) and lherzolitic to websteritic peridotite (pale brownish green to pale brown). At the boundary between these ultramafic rocks and felsic gneisses in the layered gneisses, metasomatic (metamorphic) reaction zones (up to five meters) including garnet-orthopyroxene granulites and sapphirine-bearing aluminous gneisses have been produced. Sometimes leucocratic coarse-grained garnet-bearing quartzofeldspathic rock and pale gray colored quartzose rock occur at the boudin neck of the ultramafic rocks. Strongly foliated lherzolitic peridotite block in felsic orthopyroxene gneiss is also present in Unit I, where metamorphic foliations of both ultramafic rock and surrounding felsic gneiss are clearly oblique. In addition to these ultramafic rocks, hornblende lherzolitic peridotite occurs in Unit II. The Hbl lherzolitic peridotite is oblique against the layers of the neighboring quartzo-feldspathic gneiss, suggesting that this rock was intrusive rock (Owada *et al.*, 1999).

Orthopyroxene and clinopyroxene are the main constituents of orthopyroxenite and clinopyroxenite, respectively (Plate 6A). Part of the pyroxene shows an inverted pigeonitic feature. The lherzolitic peridotite contains olivine, clinopyroxene and orthopyroxene (Plate 6B). Spinel, pale brown to colorless pargasitic hornblende, phlogopite and rarely plagioclase are also present as primary minerals. Garnet occurs only at the grain boundary between pyroxenes. The hornblende lherzolitic peridotite (sample C98012802) consists mainly of olivine (37.1 modal %), clinopyroxene (16.8 %), orthopyroxene (27.5 %) and hornblende (12.9 %), with trace amounts of spinel, magnetite and apatite. The rock is generally medium- to coarse-grained with granoblastic texture. Hornblende is medium in grain size and brown to pale brown in pleochroism. It

contains many opaque minerals. Subhedral apatite locally occurs in olivine. Hornblende is included in olivine as poikilitic inclusions. Observed mineral assemblages for the ultramafic rocks are as follows:

1) orthopyroxene + spinel + garnet + phlogopite,
2) orthopyroxene + clinopyroxene + hornblende,
3) orthopyroxene + clinopyroxene + garnet,
4) clinopyroxene + orthopyroxene + spinel,
5) clinopyroxene + orthopyroxene + phlogopite,
6) clinopyroxene + orthopyroxene + hornblende + phlogopite + spinel,
7) olivine + clinopyroxene + orthopyroxene + hornblende + phlogopite,
8) olivine + clinopyroxene + orthopyroxene + hornblende + spinel.

Magnetite, magnetite + corundum intergrowths as a breakdown of spinel and apatite are locally presence as accessory minerals.

3.9. Garnet-two pyroxene metamorphosed mafic dyke (Dm)

Distinctive metamorphosed mafic dikes with tholeiitic composition are present along shear zones, especially at the boundary between Unit II and Unit III. They cut across the foliation and layering of granulites and also fabric of the shear zone (Plate 3E). The dyke can be subdivided into two portions; 1) pale pinkish garnet-rich lens and 2) dark grayish hornblende-rich matrix. Their mineral assemblages are as follows:

1) garnet + plagioclase + orthopyroxene + clinopyroxene (with minor hornblende and quartz)
2) hornblende + plagioclase + clinopyroxene (with minor orthopyroxene, garnet and quartz)

Accessory minerals are biotite, apatite, ilmenite and magnetite. Garnet in the garnet-rich portion is generally euhedral in shape and contains inclusion of quartz and ilmenite. Orthopyroxene is dominant in the lens rather than hornblende-rich portion. Hornblende is brownish in color and occasionally coexist with clinopyroxene. The garnet-rich portion is apparently deformed and present as elongated lenses of up to 10 cm in hornblende-rich matrix. The two portions are, however, both fine-grained and granoblastic in texture. No deformation texture is present under microscopic observation. The evidence suggests an overprinting of granulite-facies metamorphism after shearing. The dykes are, however, locally mylonitized due to later deformation (Plate 7E).

3.10. Sapphirine-bearing aluminous gneiss and granulite (Gsa)

Sapphirine-bearing aluminous gneisses on Tonagh Island show various rock types and modes of occurrence as follows:

(a) A variety in mineral assemblages of sapphirine-bearing aluminous gneisses are observed as a part of garnet-orthopyroxene-bearing thin layer (up to 1 m in thickness) around ultramafic rocks, probably a metasomatic reaction zone between ultramafic and quartzo-feldspathic gneisses, in the layered gneiss of the northern peninsular area (Unit I, Plate 4A). The aluminous gneiss-bearing layer crops out intermittently over 400 m along the strike. This type of rock shows medium- to coarse-grained gneissose structure with various colors, from pale pinkish to dark brownish, due to the constituent minerals.

(b) Sapphirine-garnet-orthopyroxene-bearing aluminous gneisses occur as dark colored

lenticular or rounded blocks (several centimeters to meters in diameter) in the quartzo-feldspathic gneisses, usually surrounded by granitic leucosome, as may be derived from restite remaining after partial melting of country rocks. Commonly this type of rock is medium to coarse-grained massive granulite (Plate 4B).

(c) Phlogopite-rich sapphirine-spinel-corundum-bearing block is enclosed within the alternation of orthopyroxene felsic gneiss and two-pyroxene mafic granulite. The block show zonal structure, such as pale brown at the core part and reddish brown at the mantle due to the modal proportion and color of phlogopite (Plate 4C).

(d) Sapphirine is also contained in quartzo-feldspathic leucocratic fine- to medium-grained thin layers (several centimeters to a few meters) among layered gneiss alternating with mafic granulites, magnetite-quartz gneiss, and other sapphirine-free quartzo-feldspathic gneisses.

Sapphirine-bearing gneiss and granulite of types (a), (b) and (c) do not contain quartz, while gneiss of type (d) characteristically coexists with quartz. Observed mineral assemblages of the sapphirine-bearing aluminous metamorphic rocks are as follows:

1) sapphirine + orthopyroxene + spinel,
2) sapphirine + orthopyroxene + cordierite + spinel,
3) sapphirine + garnet + orthopyroxene,
4) sapphirine + garnet + orthopyroxene + sillimanite,
5) sapphirine + garnet + orthopyroxene + spinel,
6) sapphirine + garnet + orthopyroxene + cordierite + sillimanite,
7) sapphirine + garnet + orthopyroxene + cordierite + spinel,
8) sapphirine + garnet + orthopyroxene + spinel + corundum,
9) sapphirine + garnet + orthopyroxene + cordierite + spinel + sillimanite,
10) garnet + orthopyroxene + sapphirine,
11) garnet + orthopyroxene + spinel + sapphirine,
12) garnet + orthopyroxene + cordierite + sapphirine,
13) garnet + orthopyroxene + spinel + sillimanite + sapphirine + corundum,
14) sapphirine + spinel + corundum + phlogopite,
15) sapphirine + spinel + corundum + cordierite + phlogopite,
16) sapphirine + spinel,
17) garnet + sillimanite + sapphirine + quartz,
18) garnet + orthopyroxene + sapphirine + sillimanite + quartz,
19) garnet + orthopyroxene + sapphirine + spinel + sillimanite + quartz,
20) garnet + orthopyroxene + sapphirine + cordierite + sillimanite + quartz.

Plagioclase is contained in all these assemblages, and perthitic to mesoperthitic alkali feldspar is occasionally contained in assemblages 1) ~ 9), 12) ~ 13) and 17) ~ 20). Trace and accessory minerals are rutile, biotite, zircon, monazite, ilmenite and apatite.

Assemblages 1) ~ 9) are equivalent to type (a) including characteristically chromium-rich greenish euhedral sapphirine and chromian brownish spinel (Plate 6C). Partly symplectite intergrowths of sapphirine + orthopyroxene and sapphirine + plagioclase are also observed. Sillimanite commonly occurs as inclusions in garnet. Green spinel exists only as interstitial occurrences between orthopyroxene grains in assemblages 7) and 8), where spinel and orthopyroxene direct contact is not observed by the moat of sapphirine on the spinel side and garnet on the orthopyroxene side. In assemblage 9), cordierite + orthopyroxene + K-feldspar + quartz symplectite can also be

observed as may be the break down product of osumilite (Berg and Wheeler, 1976; Audibert *et al.*, 1993). Assemblages 10) ~ 13) correspond to type (b). Sapphirine, spinel and sillimanite are generally associated with garnet, and commonly included in garnet. Corundum is occasionally accompanied by spinel. In assemblages 10) and 11), pale-bluish sapphirine occurs only as an interstitial exsolved phase from aluminous orthopyroxene (up to 11.5 wt.% of Al_2O_3). This type of rock is characteristically poor in felsic minerals (Plate 6D). Assemblages 14) to 16) and 17) to 20) are seen in type (c) and type (d) rocks, respectively. Assemblage 14) in type (c) occurs in the block with zonal structure, where high-magnesian colorless sapphirine porphyroblast includes colorless spinel and corundum surrounded by colorless phlogopite in the core, and less-magnesian bluish sapphirine, coexisting with pale brownish phlogopite, includes green spinel and corundum at the mantle of the block (Plate 6E). Small bluish pods of sapphirine-spinel-feldspar granulite (assemblage 16) occur in the mantle part of this block. Type (d) rocks would have formed as normal UHT subsolidus reaction products, where the following reaction textures are observed: sapphirine + garnet + quartz = orthopyroxene + sillimanite or sapphirine + quartz = orthopyroxene + sillimanite + cordierite through the isobaric cooling (IBC: e.g. Harley, 1998) (Plate 6F). Detailed petrographical features of sapphirine-bearing gneisses from northern area (Units I and II) are also described in Hokada *et al.* (1999).

3.11. Impure quartzite (Q)

Medium- to coarse-grained impure quartzite occurs as thin intercalations within layered gneisses in Units I, II, III and IV (Plate 3F). The layers with milky light gray color range from several centimeters to several meters in thickness. Commonly, mineral assemblages of impure quartzite from the Napier Complex are quite variable, as has been reported by many workers (e.g. Motoyoshi and Matsueda, 1984; Motoyoshi *et al.*, 1990; Ishizuka *et al.*, 1998). Nevertheless, those from Tonagh Island are relatively simple in that quartz is the most prominent component and minor or rare plagioclase, K-feldspar, orthopyroxene and garnet are also contained (Plate 7A).

3.12. Calc-silicate granulite (Gc)

On Tonagh Island, calc-silicate granulites are found only as boulders ranging from a few centimeters to several meters in diameter around the layered gneiss area of Unit II without any moraine deposits. Therefore, these boulders could be derived from autochthonous origin. According to Sheraton *et al.* (1987), calc-silicate granulites are very rare in the Napier Complex, such as in the Khmara Bay area (diopside-plagioclase-scapolite±grossular), Mt. Gleadell (diopside-plagioclase-quartz), and the nunatak west of Mt. Bergin (diopside-plagioclase-grossular-scapolite-quartz). Wollastonite-bearing assemblages also were found only at McLeod Nunataks (Warren and Hensen, 1983), McIntyre Island (Sandiford and Wilson, 1986) and Mt. Pardoe (Osanai, unpubl.data).

Medium- to coarse-grained calc-silicate granulites from Tonagh Island are classified into three types as follows (Plate 7B):

1) diopside + grossular + quartz + plagioclase,
2) diopside + scapolite + zoisite + plagioclase + quartz,
3) diopside + wollastonite + calcite + quartz.

Accessory minerals are ilmenite, apatite and titanite.

4. Intrusive Rocks

Unmetamorphosed intrusive rocks from Tonagh Island are subdivided into three types such as alkali-dolerite (so-called Amundsen dike: Sheraton *et al.*, 1987), granitic pegmatite and lamproite. Mappable scale dikes are distributed in Units II, III, IV and V, while other small scale intrusive rocks of both types as well as aplitic rock occur throughout Tonagh Island.

4.1. Pegmatites (P)

The granitic pegmatite is mainly biotite-pegmatite containing plagioclase, K-feldspar, quartz and biotite, while part of the pegmatite is muscovite-, garnet- and tourmaline- bearing pegmatite instead of biotite (Plate 4D and 7C). Those of granitic pegmatite and aplitic rock strike mainly NE-SW with steep dip. The granitic pegmatite is not having any chilled margin. A retrograde hydration effect with amphibole formed in the host pyroxene-bearing gneisses (several centimeters in width) appears at the boundary between granitic pegmatite and adjacent country rock.

The charnockitic pegmatite also occurs as dike in Unit II. This dike cuts the neighboring metamorphic foliation of the mafic gneiss. The charnockitic pegmatite shows mylonitic foliation defined by elongated quartz and feldspars. Constituent minerals are mainly plagioclase, quartz, K-feldspar, orthopyroxene and clinopyroxene. Kink bands are locally recognized in pyroxene crystals.

4.2. Dolerite (D)

The alkali-dolerite cuts across the layered structure of the metamorphic rocks and large shear zone (Plate 4E), which is regarded as the boundary between Units II and III. Intrusive directions of the alkali-dolerite are NE-SW and WNW-ESE with a conjugate system. The width of intrusive rocks varies from a few centimeters to several meters (up to 15 m). A chilled margin of the alkali-dolerite (several centimeters in thickness) is well developed, but thin intrusions lack a distinctive chilled margin. The boundary between the alkali-dolerite and host metamorphic rocks shows no thermal effect.

Most of the alkali-dolerite dikes are black- to dark-gray-colored and massive, and display subophitic to intergranular texture. The alkali-dolerite contains phenocrysts of purplish brown clinopyroxene, plagioclase and biotite with fine-grained groundmass (clinopyroxene, plagioclase and probably green amphibole). The chilled margin of the rock is characteristically fine-grained and contains the same minerals except biotite. Accessory minerals are ilmenite, magnetite, apatite and sulfide minerals.

Clinopyroxene exhibits euhedral to subhedral shape and pale-red to pale-green with pleochroism. Plagioclase shows euhedral to subhedral shape and zoning. Biotite is locally presence as phenocrysts, and shows subhedral shape. It is reddish brown to pale brown with pleochroism.

Fine-grained green amphibole and garnet are presence in grounndmass as recrystallized minerals although the alkali-dolerite is free from UHT metamorphic episode, but cutting foliation and shear zone. Similar recrystallized minerals in the mafic dikes have been reported from the Mount Riiser-Larsen area (Ishizuka and Suzuki, 1999).

4.3. Lamproite (L)

Lamproite dykes are NS-trending, subvertical thin sheets that could be followed for a few kilometers sporadically in the southern part of Tonagh Island (Unit V). Individual bodies range from a few centimeters to one meter in thickness and up to several meters in length. The sheets cut the NE-trending gneissosity of the host rocks at high angles and are finer grained at their contacts. Some lamproite veins have metasomatized the host granulite in which primary minerals have been replaced by metasomatic phases (Miyamoto *et al.*, 2000).

The lamproite is holocrystalline and ranges from medium to dark green (Plate 4F). Some hand specimens have centimeter scale layering constituted by variations in size and proportion of minerals. The lamproite consists of microcline, potassic richterite, apatite and biotite, with trace amounts of quartz, rounded sphene and small rutile (Plate 7D). Carbonate minerals, zircon and monazite also occur as accessory minerals. Potassic richterite and microcline become finer-grained toward the margins of the lamproite dykes, whereas biotite and apatite do not. Feldspar megacrysts and autoliths up to 1.5 - 3 cm are present locally. Autoliths consists largely of the same minerals as the host dyke rock, but are coarser grained.

5. Geologic structures

The major geologic structures in Tonagh Island and East Tonagh Island are NE-SW trending foliation with WNW plunging mineral lineation, WNW-ESE to E-W trending folds and NE-SW to E-W trending mylonite zones (Figs. 3 and 4). These structures and the other minor ones were formed through the following poly-stage deformation. The deformation history of the ultrahigh-temperature metamorphic rocks is divided into nine stages, from D_1 to D_9 (largely I to IV), based on the characteristics of the deformation structures, deformation textures and movement pictures (Toyoshima *et al.*, 1999), as outlined in Table 1 and Plate 8. Deformation structures abundant in each unit are different, except for D_2 structures, as shown in Table 2 and Fig. 3.

The D_1 structure would have been formed under non- or weak-deformational condition during thermal peak of prograde metamorphism (cf. Osanai *et al.*, 1999; Hokada *et al.*, 1999; Tsunogae *et al.*, 1999). The D_2-D_6 structures would have been produced under retrograde granulite facies conditions (cf. Tsunogae *et al.*, 1999). The D_3 and D_6 fault rocks show that seismic faulting and plastic deformation alternated both during the D_3 and D_6 stages. Subsequently D_7-D_9 brittle faulting modified the structures in part. The D_1 to D_8 deformation corresponds to first to third tectonometamorphic episodes of the whole Napier Complex before the intrusion of the Amundsen dyke (Table 1) (James and Black, 1981; Sheraton *et al.*, 1987; Black, 1988; Harley and Hensen, 1990).

The D_1 structures are foliation (S_1) with very weak or no mineral lineation (L_1), symmetrical boudins with a pancake shape and a complex network of quartzo-feldspathic veins (Plate 8A). The S_1 is parallel to lithologic boundaries and compositional layering (S0) of the metamorphic rocks. Scarcely recognizable L_1 is different in orientation from post-D_1 lineations (Fig. 4). The D_1 boudins were flattened parallel to the S_1 and

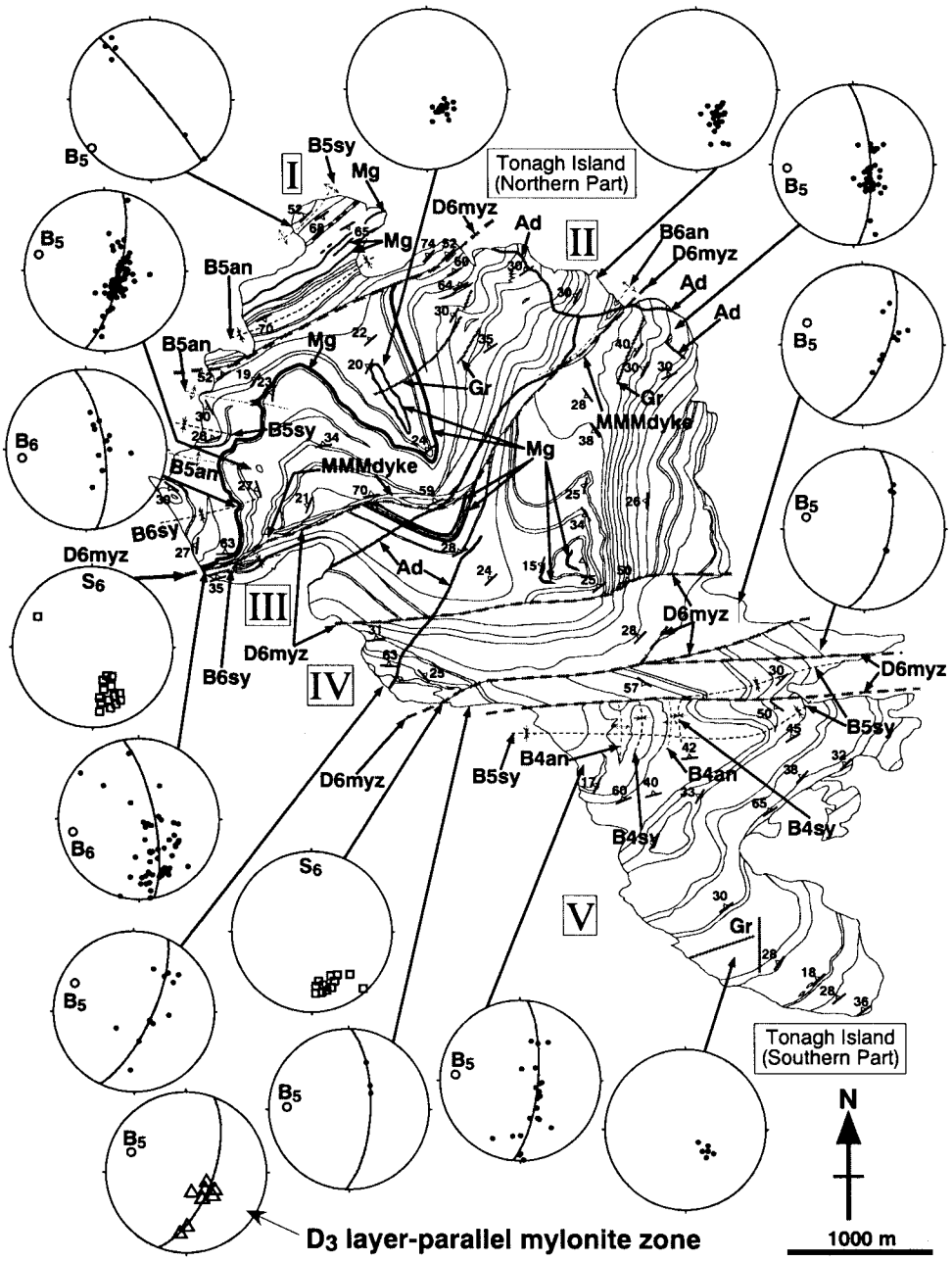

Fig. 3 Structural map and lower hemisphere equal area projections of poles to foliations (S2:●, S3:△, S6:□) and to their best fit great circles (○, B5, B6) within Tonagh Island, modified from Osanai et al. (1999). The poles (πaxis) of these great circles express stereographically the orientations of the fold axes (B5 and B6). I, II, III, IV and V: lithologic units (Osanai et al., 1999). D6myz and thick broken line: D6-mylonite zone, MMMdyke: D6-metamorphosed and mylonitized mafic dyke, thick line: dykes (Ad: Amundsen dolerite dyke (D9-dolerite dyke), Gr: D9-pegmatite dyke) or magnetite-quartz gneiss (Mg), thin broken line: fold axis (B4an: B4-antiform, B4sy: B4-synform, B5an: B5-antiform, B5sy: B5-synform, B6an: B6-antiform, B6sy: B6-synform), thin line: lithologic boundary.

Table 1. Deformation history of ultrahigh-temperature metamorphic rocks from Tonagh Island. Tectonometamorphic episodes are from Sheraton et al. (1987).*

Deformation stage		Movement picture	Deformation & structure	Metamorphism	Tectono-metamorphic episode*
I	D_0	Formation of sedimentary precursors	?	Low-grade metamorphism ?	
	D_1	?	Non-deformational - very weakly deformationary conditions but partly flattening Bedding foliation (S_1) with no mineral lineation or very weak mineral lineation (L_1) or boudinage Quartzofeldspathic vein filling up fracture	Prograde metamorphism & anatexis? Metamorphic peak over 1000°C	D_1-M_1
II	D_2	Top-to-the ESE movement (dextral-reverse faulting) ?	Shearing & intrafolial folding NE-SW to E-W trending shear plane (foliation, S_2) with WNW-ESE trending mineral lineation (L_2) WNW-ESE trending fold with axial foliation	Initiation of retrograde metamorphism?	D_2-M_2
	D_3	Top-to-the ESE movement (dextral-reverse faulting)	Shearing, folding & retrograde mylonitization (High-temperature mylonitization) NE-SW trending mylonitic foliation (S_3) with strong mineral lineation (L_3) (thin mylonite) Mylonite, pseudotachylyte & foliated pseudotachylyte	Retrograde metamorphism granulite facies	
	D_4	E-W trending compression	N-S trending gentle folding		
III	D_5	N-S trending compression	WNW-ESE to E-W trending folding Tight to gentle fold with steep axial foliation (S_5) and minor shear zone	Retrograde metamorphism	D_3-M_3
	D_6	Top-to-the ESE, WNW, NE, NW, ESE or NW movements (sinistral-normal, reverse or dextral faulting)	Retrograde mylonitization & brittle deformation NE-SW to E-W trending mylonitic foliation with NW-SE to WNW-ESE trending mineral lineation Mylonite, pseudotachylyte & foliated pseudotachylyte NE-SW to E-W trending tight to gentle drag fold Intrusion of mafic dyke (metamorphosed & mylonitized)	Retrograde metamorphism granulite facies	
IV	D_7	Dextral faulting	N-S to NNE-SSW trending vertical joint with Grt-Hbl vein & minor mylonite zone	Retrograde metamorphism amphibolite facies	
	D_8	Sinistral faulting	NE-SW trending pseudotachylyte with N-S & NW-SE trending pseudotachylyte		
	D_9	?	Fracturing with pegmatite or dolerite dykes		

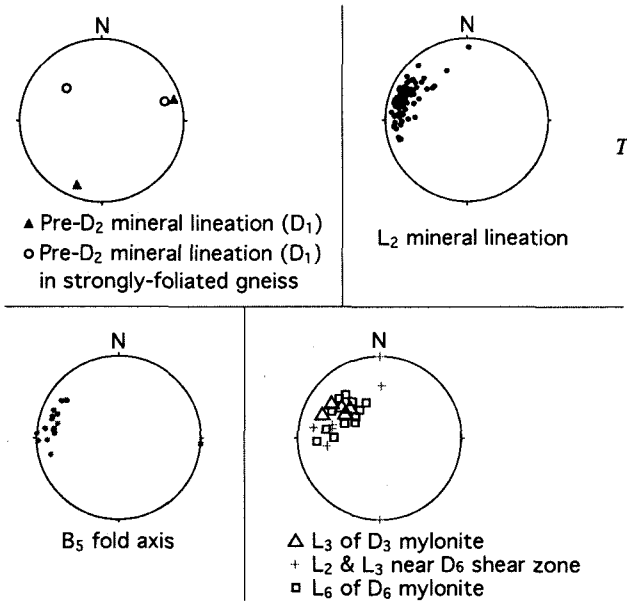

Fig. 4. Lower hemisphere equal area projections of pre-D2, D2,D3 and L6 mineral lineations and B5 fold axes within Tonagh Island.

Table 2. Deformation structures abundant in each unit.

Unit	Deformation structures
I	S1, B5
II	S2, S1, S3 Western part: B5, B6, B2
III	S2, S1 Eastern part: B5, B6
IV	S2, S1, B5
V	S2, S1, S3 Northern part: B4, B5 Eastern Tonagh Island: B2, B5

compositional layering. The D_1 structures have been mostly modified and disturbed by post-D_1 deformations, but preserved in some areas and parts (e.g. a northeastern small peninsula) of the Island (Table 2).

The D_2 structure are the NE-SW trending and NW dipping foliation (S_2) with the strong mineral lineation (L_2) (Figs. 3, 4 and Plate 8). The S_2 and L_2 structures are prominent ones in the Tonagh metamorphic rocks and are associated with asymmetrical rotated boudinage and asymmetrical intrafolial fold (B_2) with well-developed axial foliation (S_2') (Plate 8B). The D_2 structures are disturbed by D_5 to D_6 folding especially in East Tonagh Island (cf. Harley, 1987) and the western and eastern parts of Tonagh Island (Fig. 3, Table Table 2).

The D_3 structures are thin shear zones parallel or oblique to S_2 of surrounding gneiss (Plate 8C and D). The D_3 shear zone consists mainly of anhydrous mylonite with pseudotachylyte and foliated pseudotachylyte (Plate 8D). The D_3 pseudotachylyte-generating fault surfaces are parallel to S_2 of the surrounding gneiss and to the S_2-parallel D_3 mylonite zone. The S_3 of the foliated pseudotachylyte is continuous with and parallel to that of the D_3 mylonite.

The D_4 structures are geological-map scale antiforms and synforms (B_4) with N-S trending subhorizontal fold axis and subvertical axial plane in the southern part of Tonagh Island. The B_4 folds form open to gentle shapes and have been refolded by post-D_4 folding (Fig. 3).

The D_5 structure is the above-mentioned WNW-ESE to E-W trending folds (B_5) (Figs. 6.1 and 6.3E). The B_5 folds form tight to gentle shapes with subvertical to steep axial foliation (S_5) that is inclined to the pre-existing foliation (Plate 8E). The folds with small interlimb angles are associated with minor shear zones at their fold limbs. The folds

in the eastern and western parts of the island are geological-map scale antiforms and synforms (Fig. 3).

The D_6 structures are the above-mentioned NE-SW to E-W trending and steeply NW to N dipping thick mylonite zones, accompanied by drag folds (B_6) (Fig. 3 and Plate 8F). Most of the D_6 mylonite zones occur along the unit boundary faults between lithologic units (Osanai *et al.*, 1999; Toyoshima *et al.*, 1999). A D_6 mylonite zone also occurs in Unit V (Fig. 3). The D_6 mylonite zones cut pre-D_6 structures and consist of anhydrous mylonite with pseudotachylyte and foliated pseudotachylyte. The D_6 mylonites and D_6 foliated pseudotachylytes show strong mylonitic foliation (S_6) and mineral lineation (L_6) (Plate 7E and F). The L_6 lineations are parallel, oblique or perpendicular to the dip of the S_6. The mylonite zones have resulted from multiphase faulting in different shear senses during the D_6 stage. Mylonitized and metamorphosed mafic dykes intrude into the thickest mylonite zone (Fig. 3).

The B_6 drag folds, which develop near and in the D_6 mylonite zones (unit boundary faults), form isoclinal to gentle shapes with subvertical axial foliation ($S_{6'}$). Many folds are of asymmetric type; some folds show rootless forms. Some of the B_6 folds are geological-map scale antiforms and synforms (Fig. 3).

The D_7 brittle structures are N-S to NNE-SSW trending vertical faults (F_7) and joints (J_7), associated with garnet+hornblende veins and thin mylonite zones consisting of garnet+hornblende+plagioclase.

The D_8 structure is NE-SW trending pseudotachylyte zones with N-S and WNW-ESE trending pseudotachylyte zones.

Pegmatite and dolerite dykes are the products of the D_9 stage, cutting across pre-D_9 structures (Fig. 3). After the D_9 stage, no deformation took place on Tonagh Island.

6. Geochronology

The geochronological data of whole-rocks and minerals from Tonagh Island are summarized in Table 3. All data were obtained from samples collected by geological parties of Japanese Antarctic Research Expedition. These age data range from Paleozoic to Archaean.

The oldest age given by Sm-Nd whole-rock isochron method using the mafic gneisses collected from Unit I is 3714 ± 294 Ma with 0.50794 ± 0.00025 as Nd initial ratio (NdI). Individual sample corrected by the isochron age corresponds to ε_{Nd} = 1.3 to 3.4. These values resemble those of depleted mantle and widely reported basaltic and komatiitic rocks at that time (Owada *et al.*, 1994). Therefore, protolith of the mafic gneisses were separated from the depleted mantle c. 3700 Ma. In other words, the age of c. 3700 Ma can indicate crustal formation of Tonagh Island.

The felsic gneisses contain abundant zircons. Shiraishi *et al.* (1997) conducted U-Pb SHRIMP analyses for zircon in the felsic gneiss from the island. According to their results, CL and BSE images of the zircons reveal internal complexities with structurally discrete centers (inherited) rimmed by the more dominant metamorphic overgrowths. Three areas of inherited core record Archaean $^{207}Pb/^{206}Pb$ ages of about 3280 Ma, 3230 Ma and 2660 Ma, respectively. On the other hand, analytical data of

Table 3. Ages of the metamorphic and intrusive rocks from Tonagh Island.

Method	Rock type	Age	Sample No.	ref.
Sm-Nd whole rock isochron	Mafic gneiss	3708±533 Ma (IR: 0.50794±0.00046) (εNd(T): 1.3～3.3)	A90021602A A90021602AB A90021602AW A90021602C A90021603C	1
	Mafic gneiss	3714±294 Ma (IR: 0.50794±0.00025) (εNd(T): 1.3～3.4)	A90021602A A90021602AB A90021602AW A90021602Z1 A90021602Z2 A90021602C A90021602C2 A90021603C	2
	Felsic gneiss & Utramafic gneiss	2458±60 Ma (IR: 0.50897±0.00004) (εNd(T): -9.8～-9.2)	A90021603E A90021603H A90021603I A90021603N	1
	Felsic gneiss	2481±80 Ma (IR: 0.50897±0.00006) (εNd(T): -9.1～-8.1)	A90021601D A90021603A A90021603AL A90021603B A90021603D A90021603E A90021603H A90021603I	2
Sm-Nd internal isochron	Grt-Opx gneiss (Grt-Opx-whole rock)	1557±37 Ma (IR: 0.50971±0.00010) (εNd(T): -20.7)	A90021604G	2
	Spr-Grt gneiss (Grt-Spr-feldsic fraction-whole rock)	1876±61 Ma (IR: 0.50949±0.00017) (εNd(T): -14.1)	A98021801	3
	Grt feldspathic gneiss (Grt-whole rock)	1897 Ma (IR: 0.50946) (εNd(T): -14.2)	A90021603B	2
U-Pb SHRIMP	Grt feldspathic gneiss	z-c: 3230-3280 Ma z-c: 2660 Ma z-c&-r: ～2440-2550 Ma	A90021603D	4
Rb-Sr internal isochron	lamproite dike (Bt-Rt-felsic fraction-whole rock)	466±4 Ma (IR: 0.70949±0.00010)	TM990113-01A	5
	lamproite dike (Bt-Rt-felsic fraction-whole rock)	476±6 Ma (IR: 0.70966±0.00010)	TM990113-01F	5
	pegmatite (Ms-felsic fraction)	492 Ma (reference age) (IR: 0.7102±0.0071)	TM990119-03A	6

1: Owada *et al* . (1994), 2: Owada *et al* . (unpublish data), 3: Osanai *et al* . (unpublish data)
4: Shiraishi *et al* . (1997), 5: Miyamoto *et al* . (2000), 6: Miyamoto (unpublish data)
z: zircon, c: core, r: rim

outer rims yield ages from 2440 to 2550 Ma.

Sm-Nd whole-rock isochron ages of felsic and ultramafic gneisses and felsic gneiss yield ages of 2458 ± 60 Ma and 2481 ± 80Ma, respectively. U-Pb SHRIMP ages for the felsic gneiss shows 2440 to 2550 Ma (Shiraishi *et al.*, 1997). These ages are identical with the range of experimental error. Epsilon NdI values corrected by the isochron ages for the individual samples of the felsic gneisses have -9.8 to -8.1. These values are extremely low compared with that of CHUR (chondrite uniform reservoir). The large negative εNdI values obtained from felsic gneisses suggest that these rocks have a long time crustal history before c. 2500 Ma.

Hokada (1999) performed chemical dating method of monazite and zircon involving UHT assemblage metamorphic rocks in the Mt. Riiser-Larsen region. In the sapphirine-osumilite bearing layer in the garnet-orthopyroxene quartzo-feldspathic gneiss, the monazite and zircon grains embedded within osumilite give ages of c. 2500 Ma. This indicates that the monazite and zircon grains have crystallized during UHT metamorphism. Similar ages have been reported for the rocks from almost entire the Napier Complex (DePaolo *et al.*, 1982; Black *et al.*, 1983; McCulloch and Black, 1984; Black *et al.*, 1986b; Tainosho *et al.*, 1994; Harley and Black, 1997; Asami *et al.*, 1998; Hokada, 1999; Suzuki, 2000). Therefore, the whole-rock isochron age of c. 2500 Ma for the felsic gneisses would reflects isotopic equilibration due to major tectonothermal event of UHT in the Napier Complex.

Sm-Nd mineral isochron ages were obtained from garnet quartzo-feldspathic gneiss, sapphirine-bearing garnet-orthopyroxene gneiss and garnet-orthopyroxene gneiss. The former two yield isochron ages of 1897 Ma and 1876 ± 61 Ma, respectively. On the other hand, garnet-orthopyroxene gneiss gives an isochron age of 1557 ± 37 Ma. These ages are apparently younger than that of major tectonothermal event involving UHT metamorphism, suggesting that there would be at least two tectonothermal events followed by UHT metamorphism during the middle Proterozoic time.

The approximate ages of the igneous activities the alkali-dolerite is considered to be c.1200 Ma (Sheraton and Black, 1981) and for the granitic pegmatite is 500-550 Ma (Black et al., 1983). Rb-Sr internal isochrons determined from biotite-poor and biotite-rich lamproites gave, respectively, ages of 476 ± 6 Ma and 466 ± 4 Ma with initial ratios of 0.70966 ± 0.00010 and 0.70949 ± 0.00010 (Miyamoto *et al.*, 2000). An internal Rb-Sr isochron age for muscovite-bearing aplitic pegmatite from Unit II of Tonagh Island is also determined here using mesh partitioned plagioclase, K-feldspar and muscovite. Result is not exactly confirmed yet, but reference isochron gave an age of 492 Ma.

7. Geochemistry

Representative bulk chemical data for the metamorphic rocks from Tonagh Island are listed in Table 4. Here we briefly explain only for mafic, ultramafic and sapphirine-bearing metamorphic rocks and unmetamorphosed dolerite dike. Chemical compositions of other rock types are just showing in Table 4 and Fig. 5. Garnet- and orthopyroxene-bearing felsic gneisses, two pyroxene-bearing mafic granulite and ultramafic granulite could be derived from Archaean TTG-type felsic igneous rock, mafic

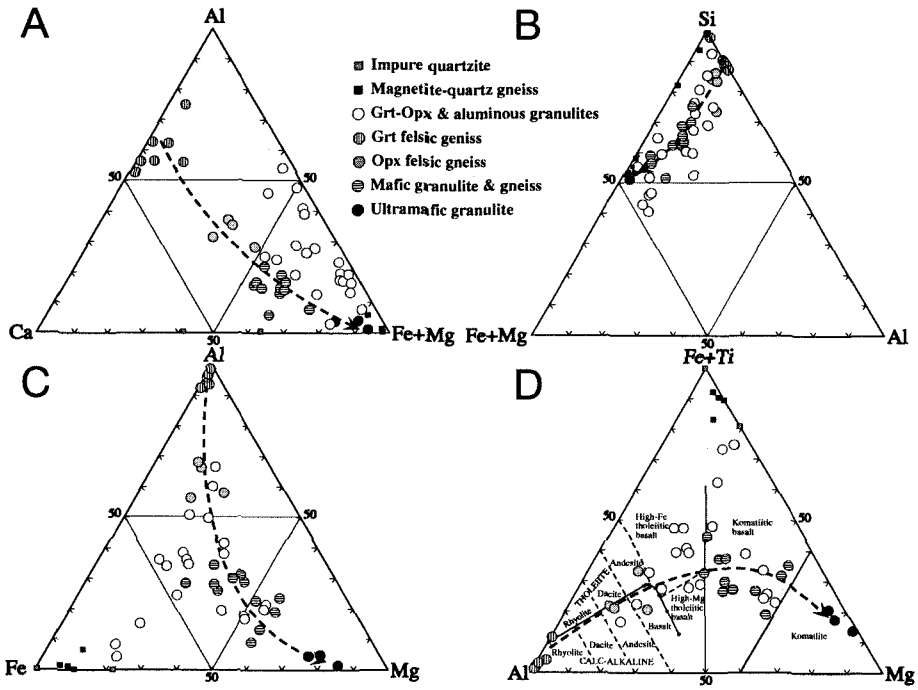

Fig. 5 Bulk rock chemistries of the metamorphic rocks from Tonagh island. A: Al - Ca - (Fe+Mg) plot. B: Si - (Fe+Mg) - Al plot. C: Al - Fe - Mg plot. D: (Fe+Ti) - Al - Mg plot.

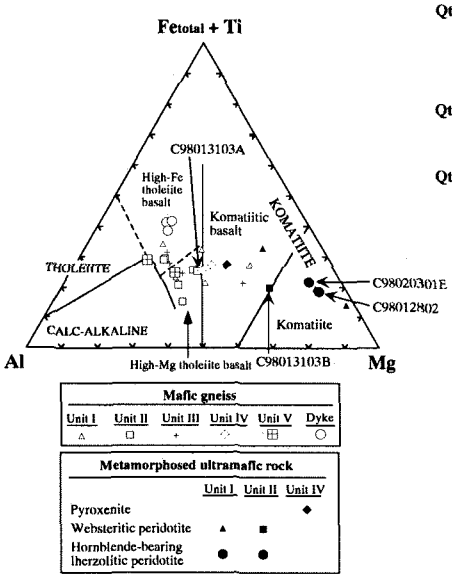

Fig. 6 (Fe_{total}+Ti) - Al - Mg diagram (Jensen, 1976) for the mafic and ultramafic granulites from Tonagh Island.

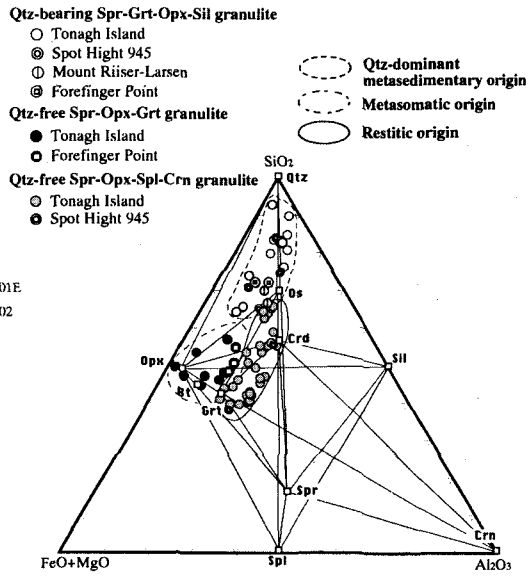

Fig. 7 Si - (Fe+Mg) - Al diagram for the sapphirine-bearing aluminous gneisses from Tonagh Island.

Table 4. Bulk rock analyses of the metamorphic and itrusive rocks from Tonagh Island.

Rock type	Gof						Ggf	Gm									Ggo		
								BHPG	BHPG	BHPG	BHPG	PG	PG	BPG	BPG	PG	GO-gn	GO-gr	GCS
Sample No.	C9801-2801A	C9801-2902A	C9801-2904D	C9802-0804F	C9802-0901	C9802-2201D	A9002-1603D	A9002-1601G	A9002-1602C	C9801-2801B	C9801-3103A	C9802-1003H	C9802-0902F	C9802-1104F	C9801-3002F	C9802-2202C	A9002-1603B	A9002-1604G	A9002-1604E
Unit	Unit II	Unit II	Unit II	Unit III	Unit III	Unit V	Unit I	Unit I	Unit I	Unit II	Unit II	Unit II	Unit III	Unit III	Unit IV	Unit V	Unit I	Unit I	Unit I
wt %																			
SiO_2	82.42	57.90	59.25	76.50	72.18	68.67	73.75	54.82	50.36	50.48	47.06	50.46	52.70	54.50	45.07	49.84	56.69	49.08	52.43
TiO_2	0.22	1.06	0.78	0.06	0.46	0.64	0.28	0.45	1.11	0.92	0.41	0.62	0.75	0.59	0.98	0.69	1.17	0.35	0.36
Al_2O_3	10.43	16.56	15.30	14.17	14.25	14.24	11.44	12.86	8.72	16.08	19.14	12.89	14.56	9.76	15.09	15.31	16.57	2.94	19.92
Fe_2O_3	1.93	8.86	8.78	0.89	3.18	5.98	8.04	10.59	15.03	10.42	9.30	12.74	12.29	11.15	15.27	12.44	12.51	33.84	15.66
MnO	0.01	0.11	0.12	0.01	0.03	0.07	0.19	0.17	0.23	0.14	0.12	0.22	0.17	0.14	0.23	0.23	0.20	1.88	0.93
MgO	0.19	5.24	5.13	0.42	0.96	2.00	2.61	10.51	14.76	8.82	11.40	9.35	8.55	13.95	11.87	7.82	4.47	5.24	5.81
CaO	1.60	5.70	6.35	2.89	2.90	3.55	2.03	8.87	8.10	11.35	11.18	12.22	7.42	5.81	9.51	14.49	5.75	6.60	2.40
Na_2O	3.89	3.29	3.68	3.15	3.60	3.75	1.18	2.03	1.17	2.36	1.48	1.92	3.05	1.93	0.53	0.67	1.62	0.00	1.03
K_2O	0.65	0.36	0.81	2.62	2.80	1.17	0.49	0.40	1.03	0.31	0.17	0.22	0.53	1.50	1.38	0.13	0.91	0.00	1.45
P_2O_5	0.00	0.08	0.07	0.01	0.07	0.05	0.00	0.08	0.26	0.12	0.02	0.05	0.07	0.30	0.06	0.12	0.12	0.06	0.02
ppm																			
Ba	650*	355*	220*	1390*	1170*	590*	198.7	61	259	91	39	46	175	828	165	23	262.3	10	512.7
Co	nd.	nd.	nd.	nd.	nd.	nd.	nd.	48	76	55	nd.	53	46	43	56	48	nd.	32	nd.
Cr	<5*	166*	178*	8*	14*	27/*	347.7	736	1800	505	247*	1190	623	1170	286	607	146.8	136.4	506.8
Cu	nd.	nd.	nd.	nd.	nd.	nd.	nd.	16	51	73	nd.	19	29	<10	59	<10	nd.	nd.	nd.
Nb	3*	15*	12*	4*	8*	13*	5	2.9	4.7	4.3	1.3	4.8	6.3	4.5	2.3	4.0	15	20	5
Ni	19*	156*	55*	34*	19*	49*	50	198	680	234	372*	121	95	143	131	102	94.1	150	43.9
Rb	7*	3*	5*	35*	30*	6*	6	10	36	2	<2*	5	4	124	25	2	12	5	43
Sr	110*	173*	143*	187*	268*	225*	68.5	69	120	152	130*	57	108	240	61	103	132.4	6	55.7
V	7*	190*	171*	5*	57*	116*	68.7	217	157	210	103*	239	209	143	286	218	215.7	86	139.6
Y	<2*	36*	26*	<2*	15*	19*	300	20	27	36	10	30	32	22	18	45	50	20	55
Zn	12*	70*	81*	13*	42*	78*	nd.	94	91	60	63*	106	122	74	82	82	nd.	4	nd.
Zr	308*	183*	118*	66*	109*	140*	540	86	108	75	25	61	81	126	40	35	95	20	185
Ga	nd.	nd.	nd.	nd.	nd.	nd.	nd.	15	15	17	nd.	15	16	14	16	17	nd.	6	nd.

*: trace elements determined with XRF, other data analyzed by ICP-MS

Table 3. (continued)

Sample No.	C9801-2801A	C9801-2902A	C9801-2904D	C9802-0804F	C9802-0901	C9802-2201D	A9002-1603D	A9002-1601G	A9002-1602C	C9801-2801B	C9801-3103A	C9802-1003H	C9802-0902F	C9802-1104F	C9801-3002F	C9802-2202C	A9002-1603B	A9002-1604G	A9002-1604E
La	nd.	nd.	nd.	nd.	nd.	nd.	29.0	10.90	17.30	13.40	2.95	12.90	22.60	28.40	3.17	7.79	60.0	4.0	14.0
Ce	nd.	nd.	nd.	nd.	nd.	nd.	85.0	23.30	37.40	29.00	6.44	31.20	43.20	58.30	8.00	24.50	130.0	12.0	24.0
Pr	nd.	nd.	nd.	nd.	nd.	nd.	nd.	2.61	4.23	3.27	0.81	3.60	4.45	6.22	1.09	3.58	nd.	nd.	nd.
Nd	nd.	nd.	nd.	nd.	nd.	nd.	10	11.30	19.20	15.00	4.10	14.80	18.10	26.80	5.99	18.60	40	5.1	<5
Sm	nd.	nd.	nd.	nd.	nd.	nd.	5.30	2.98	4.97	4.37	1.20	3.96	4.25	5.94	1.94	6.73	8.60	1.50	3.50
Eu	nd.	nd.	nd.	nd.	nd.	nd.	1.00	0.661	1.570	1.100	0.520	0.803	1.110	1.260	0.869	2.450	1.50	0.3	0.45
Gd	nd.	nd.	nd.	nd.	nd.	nd.	nd.	3.10	4.97	4.71	1.44	4.38	4.65	5.26	2.31	7.39	nd.	nd.	nd.
Tb	nd.	nd.	nd.	nd.	nd.	nd.	3.20	0.53	0.83	0.89	0.27	0.80	0.80	0.71	0.46	1.49	1.50	0.50	1.10
Dy	nd.	nd.	nd.	nd.	nd.	nd.	nd.	3.43	4.92	5.89	1.60	5.04	5.00	3.95	2.97	8.45	nd.	nd.	nd.
Ho	nd.	nd.	nd.	nd.	nd.	nd.	nd.	0.74	1.01	1.28	0.34	1.06	1.10	0.76	0.68	1.55	nd.	nd.	nd.
Er	nd.	nd.	nd.	nd.	nd.	nd.	nd.	2.15	2.75	3.79	0.91	3.15	3.44	2.18	2.06	4.01	nd.	nd.	nd.
Tm	nd.	nd.	nd.	nd.	nd.	nd.	nd.	0.318	0.384	0.574	0.140	0.471	0.541	0.309	0.330	0.541	nd.	nd.	nd.
Yb	nd.	nd.	nd.	nd.	nd.	nd.	38.80	1.98	2.23	3.35	0.95	2.69	3.25	1.87	1.97	2.92	4.40	0.90	5.00
Lu	nd.	nd.	nd.	nd.	nd.	nd.	5.70	0.273	0.337	0.466	0.150	0.386	0.477	0.246	0.299	0.322	0.60	0.10	0.70
Hf	nd.	nd.	nd.	nd.	nd.	nd.	nd.	2.2	3.0	1.8	0.7	1.7	2.3	3.1	1.2	1.3	nd.	nd.	nd.
Ta	nd.	nd.	nd.	nd.	nd.	nd.	nd.	0.3	0.4	0.3	0.2	0.5	0.7	0.4	0.2	0.5	nd.	nd.	nd.
Th	nd.	nd.	nd.	nd.	nd.	nd.	nd.	0.73	1.92	3.62	0.01	5.89	2.21	4.67	0.16	1.08	nd.	nd.	nd.
U	nd.	nd.	nd.	nd.	nd.	nd.	nd.	0.30	0.52	0.76	0.00	1.30	0.70	2.02	0.06	0.35	nd.	nd.	nd.

BHPG; brown hornblende two pyroxene mafic gneiss
PG; two pyroxene mafic gneiss
BPG; biotite-bearing two pyroxene mafic gneiss
GO-gn; garnet-orthopyroxene gneiss
GO-gr; garnet-orthopyroxene granulite
GCS; Garnet-cordierite-sillimanite gneiss

Analyticdal data are after Owada *et al* . (1999) and Osanai (unpublished data).

Table 3. (continued)

Rock type	Gmq	Gu			Dm		Gsa									Q	D	
		WP	WP	HLP			SGO	SG	SGO	PhSSC	SP	SGO	SGO	SQ	SQ			
Sample No.	A9002-1701F	A9002-1603C	C9801-3103B	C9801-2802	C9802-1101A	C9802-1101G	A9002-1701G	A9802-1003B	A9802-1003I	A9801-3107A	A9801-3107B	A9002-1801F	B9802-1003C	A9802-1707B	C9802-1003C	A9002-1701A1	C9801-2803C	C9801-2901F
Unit	Unit I	Unit I	Unit II	dike	dike	dike	Unit I	Unit I	Unit I	Unit II	Unit II	Unit II	Unit II	Unit I	Unit II	Unit I	dike	dike
wt %																		
SiO_2	54.29	53.30	42.33	43.95	48.77	49.53	41.54	39.11	45.03	36.80	37.17	38.90	42.22	76.55	78.44	99.46	49.29	49.27
TiO_2	0.02	0.33	0.37	0.51	2.01	1.78	1.41	0.41	0.88	1.66	0.08	0.69	1.11	0.49	0.41	0.01	2.13	2.07
Al_2O_3	0.05	3.49	10.58	4.30	12.46	12.74	16.16	32.89	27.52	24.20	41.92	20.60	15.48	14.53	11.22	0.00	13.54	13.75
Fe_2O_3	41.73	12.24	15.16	15.14	18.21	17.04	20.85	9.09	8.42	5.31	4.26	16.19	17.64	1.74	3.95	0.35	14.75	14.45
MnO	0.18	0.21	0.20	0.20	0.28	0.27	0.25	0.18	0.12	0.04	0.07	0.27	0.40	0.01	0.01	0.01	0.20	0.19
MgO	2.76	23.71	23.22	31.05	4.59	5.09	18.34	11.24	8.72	22.57	9.21	20.70	18.35	2.27	3.47	0.00	6.09	6.41
CaO	0.81	6.84	6.19	4.97	8.39	9.01	1.28	3.31	5.00	0.01	2.38	2.23	0.69	0.62	0.26	0.17	9.10	9.55
Na_2O	0.00	0.32	0.51	0.36	2.31	2.31	0.00	2.10	2.88	0.31	4.13	0.00	0.13	1.84	0.33	0.00	2.20	1.96
K_2O	0.00	0.00	0.17	0.06	1.01	0.83	0.00	0.64	0.49	9.06	0.73	0.35	3.85	1.94	1.89	0.00	0.98	0.85
P_2O_5	0.15	0.04	0.03	0.02	0.21	0.18	0.17	0.01	0.02	0.03	0.04	0.07	0.10	0.02	0.02	0.00	0.23	0.21
ppm																		
Ba	10	9	18	4	260*	241	58.2	81*	249*	486*	137*	29.7	41*	373*	926*	10	260*	259
Co	2	96	nd.	nd.	nd.	53	nd.	nd.	nd.	nd.	nd.	nd.	nd.	nd.	nd.	2	nd.	52
Cr	104.7	5170	1139*	2142*	13*	60	92.1	2130*	1343*	60*	36*	200	62*	414*	34*	69.6	50*	77
Cu	nd.	62	nd.	nd.	nd.	85	nd.	nd.	nd.	nd.	nd.	nd.	nd.	nd.	nd.	nd.	nd.	100
Nb	5	0.8	2.0	8.6	7	6.2	5	2*	7*	50*	9*	5	13*	12*	35*	nd.	17	13
Ni	86	676	1147*	1786*	16*	42	152	371*	198*	55*	77*	224.2	119*	147*	49*	54	48*	78
Rb	5	<2	<2*	6*	24*	17	1	10*	4*	379*	18*	6	102*	29*	26*	5	27*	21
Sr	20	5	20*	36*	208*	178	14.4	32*	106*	3*	23*	23.3	6*	47*	10*	2	434*	353
V	14	124	149*	199*	459*	403	490	249*	187*	158*	26*	242.8	162*	94*	15*	2	362*	345
Y	70	11	13	12	98*	37	35	3*	3*	173*	93*	25	91*	6*	71*	nd.	57*	26
Zn	2	123	146*	87*	137*	149	nd.	72*	36*	84*	53*	nd.	168*	47*	9*	2	114*	100
Zr	40	36	39	48	162*	145	60	720*	771*	337*	42*	70	188*	218*	639*	nd.	138*	128
Ga	2	7	nd.	nd.	nd.	22	nd.	nd.	nd.	nd.	nd.	nd.	nd.	nd.	nd.	2	nd.	21

*: trace elements determined with XRF, other data analyzed by ICP-MS

Table 3. (continued)

Sample No.	A9002-1701F	A9002-1603C	C9801-3103B	C9801-2802	C9802-1101A	C9802-1101G	A9002-1701G	A9802-1003B	A9802-10031	A9801-3107A	A9801-3107B	A9002-1801F	B9802-1003C	A9802-1707B	C9802-1003C	A9002-1701A1	C9801-2803C	C9801-2901F
La	2.0	6.19	1.72	5.35	nd.	15.9	2.0	nd.	nd.	nd.	nd.	7.0	nd.	nd.	nd.	<1.0	nd.	19.8
Ce	4.0	15.60	5.16	13.74	nd.	35.9	4.0	nd.	nd.	nd.	nd.	14.0	nd.	nd.	nd.	<2.0	nd.	45.2
Pr	nd.	1.74	0.78	1.78	nd.	4.39	nd.	nd.	nd.	nd.	nd.	nd.	nd.	nd.	nd.	nd.	nd.	5.21
Nd	<5	7.41	4.35	8.88	nd.	21.8	<5	nd.	nd.	nd.	nd.	5	nd.	nd.	nd.	<5	nd.	24
Sm	0.50	1.59	1.30	2.22	nd.	5.71	2.30	nd.	nd.	nd.	nd.	2.10	nd.	nd.	nd.	0.1	nd.	5.76
Eu	0.50	0.331	0.420	0.670	nd.	1.81	0.3	nd.	nd.	nd.	nd.	0.50	nd.	nd.	nd.	0.50	nd.	1.98
Gd	nd.	1.78	1.57	2.32	nd.	6.17	nd.	nd.	nd.	nd.	nd.	nd.	nd.	nd.	nd.	nd.	nd.	5.51
Tb	0.60	0.29	0.32	0.39	nd.	1.07	0.70	nd.	nd.	nd.	nd.	2.00	nd.	nd.	nd.	0.1	nd.	0.82
Dy	nd.	1.84	1.88	2.13	nd.	6.59	nd.	nd.	nd.	nd.	nd.	nd.	nd.	nd.	nd.	nd.	nd.	4.8
Ho	nd.	0.38	0.41	0.41	nd.	1.37	nd.	nd.	nd.	nd.	nd.	nd.	nd.	nd.	nd.	nd.	nd.	0.95
Er	nd.	1.15	1.16	1.06	nd.	4.09	nd.	nd.	nd.	nd.	nd.	nd.	nd.	nd.	nd.	nd.	nd.	2.61
Tm	nd.	0.178	0.190	0.160	nd.	0.625	nd.	nd.	nd.	nd.	nd.	nd.	nd.	nd.	nd.	nd.	nd.	0.366
Yb	0.50	1.01	1.32	0.99	nd.	3.65	2.50	nd.	nd.	nd.	nd.	2.80	nd.	nd.	nd.	0.20	nd.	2.14
Lu	0.10	0.151	0.220	0.150	nd.	0.506	0.40	nd.	nd.	nd.	nd.	0.40	nd.	nd.	nd.	<0.10	nd.	0.297
Hf	nd.	0.9	0.9	1.7	nd.	4.1	nd.	nd.	nd.	nd.	nd.	nd.	nd.	nd.	nd.	nd.	nd.	4.0
Ta	nd.	0.1	0.3	1.0	nd.	0.5	nd.	nd.	nd.	nd.	nd.	nd.	nd.	nd.	nd.	nd.	nd.	1.0
Th	nd.	1.13	0.11	1.53	nd.	1.60	nd.	nd.	nd.	nd.	nd.	nd.	nd.	nd.	nd.	nd.	nd.	2.26
U	nd.	0.36	0.02	0.43	nd.	0.39	nd.	nd.	nd.	nd.	nd.	nd.	nd.	nd.	nd.	nd.	nd.	0.48

WP; websteritic peridotite
HLP; hornblende-bearing lherzolitic peridotite
SGO; Sapphirine-garnet-orthopyroxene granulite
SG; Sapphirine-garnet granulite
PhSSC; Phlogopite-sapphirine-spinel-corundum granulite
SP; Sapphirine-plagioclase granulite
SQ; Sapphirine-quartz gneiss

Table 5. Representative electron microprobe analyses of constituent minerals.

Mineral	Orthopyroxene						Clinopyroxene			Garnet				Sapphirine		Spinel		Plagioclase				Amp	Bt
Sample No.	A9002-1702B	B9801-2802D	A9002-17GA	C9801-2802	A9801-2902D	B9802-1108A	B9801-2802D	C9801-2802	B9802-1108A	A9002-1603D	A9002-17GA	A9801-2902D	B9802-1108A	A9801-2902D	A9801-3107A	A9002-17GA	A9801-3107A	A9002-1702B	B9801-2802D	A9801-2902D	B9802-1108A	B9802-1108A	A9801-3107A
Rock type	Gof	Gm	Ggo	Gu	Gsa	Dm	Gm	U	Ggm	Ggf	Ggo	Gsa	Dm	Gsa	Gsa	Ggo	Gsa	Gof	Gm	Gsa	Ggm	Dm	Gsa
SiO_2 (wt %)	50.68	52.13	49.40	54.92	49.69	51.45	51.34	51.93	51.22	40.00	41.11	40.54	38.17	14.93	12.89	0.00	0.01	56.39	55.08	64.66	61.05	41.61	40.93
TiO_2	0.08	0.04	0.07	0.36	0.12	0.03	0.27	1.07	0.18	0.00	0.03	0.01	0.01	0.10	0.02	0.00	0.00	0.02	0.02	0.02	0.01	1.87	1.92
Al_2O_3	0.94	1.30	11.29	3.78	10.55	0.51	2.42	4.46	1.86	22.40	23.55	23.25	20.87	59.55	64.23	63.28	64.55	26.91	27.32	21.81	25.83	11.45	13.92
Cr_2O_3	0.00	0.02	0.04	0.20	0.00	0.00	0.05	0.06	0.06	0.00	0.04	0.00	0.00	0.00	0.00	0.00	0.00	0.00	0.01	0.00	0.00	0.00	0.00
FeO*	30.48	25.30	12.61	11.37	15.44	32.07	9.87	3.83	13.47	24.00	17.71	22.13	30.41	8.73	6.14	20.20	22.41	0.07	0.12	0.00	0.16	18.87	4.38
MnO	0.59	0.27	0.15	0.23	0.05	0.22	0.20	0.00	0.15	0.00	0.37	0.15	0.93	0.05	0.04	0.00	0.36	0.00	0.03	0.00	0.01	0.01	0.04
ZnO	0.00	0.00	0.00	0.00	0.08	0.12	0.02	0.00	0.00	0.00	0.00	0.00	0.05	0.01	0.00	0.94	0.89	0.00	0.00	-	0.00	0.00	0.00
MgO	16.54	19.40	26.67	29.22	24.00	15.77	12.56	15.36	10.39	13.20	16.62	14.02	3.06	16.47	16.86	15.32	11.93	0.00	0.02	0.00	0.01	8.16	24.25
CaO	0.50	0.91	0.05	0.09	0.00	0.39	22.19	23.04	21.54	0.30	1.07	0.40	7.20	0.00	0.02	0.00	0.01	9.40	9.91	2.70	7.71	11.37	0.00
Na_2O	0.00	0.00	0.00	0.02	0.00	0.04	0.49	0.60	0.56	0.00	0.00	0.00	0.00	0.03	0.00	0.00	-	6.01	5.94	9.81	6.80	1.40	0.30
K_2O	0.00	0.06	0.00	0.00	0.00	0.05	0.00	0.00	0.04	0.00	0.00	0.00	0.00	0.00	0.00	0.00	0.00	0.22	0.29	0.39	0.29	2.15	10.65
F																							5.26
-O																							-2.21
Total	99.81	99.43	100.28	100.19	99.93	100.65	99.41	100.35	99.47	99.90	100.50	100.50	100.70	99.87	100.20	99.74	100.16	99.02	98.74	99.39	101.87	96.89	99.44
cations	O=6						O=6			O=12				O=20		O=4		O=8				O=23	O=22
Si	1.970	1.981	1.750	1.931	1.784	1.993	1.940	1.890	1.963	3.006	2.990	2.993	3.018	1.784	1.519	0.000	0.000	2.556	2.515	2.857	2.670	6.418	5.759
Ti	0.002	0.001	0.002	0.010	0.003	0.001	0.008	0.029	0.005	0.000	0.002	0.001	0.001	0.009	0.002	0.000	0.000	0.001	0.001	0.001	0.000	0.216	0.203
Al	0.043	0.058	0.471	0.157	0.446	0.023	0.108	0.191	0.084	1.984	2.019	2.023	1.945	8.388	8.922	1.959	2.005	1.438	1.470	1.136	1.331	2.081	2.308
Cr	0.000	0.001	0.001	0.006	0.000	0.000	0.002	0.002	0.002	0.000	0.002	0.000	0.000	0.000	0.000	0.000	0.000	0.000	0.000	0.000	0.000	0.000	0.000
Fe	0.991	0.804	0.373	0.334	0.463	1.039	0.312	0.117	0.432	1.508	1.077	1.366	2.010	0.872	0.605	0.444	0.494	0.003	0.005	0.000	0.006	2.433	0.515
Mn	0.019	0.009	0.004	0.007	0.002	0.007	0.006	0.000	0.005	0.000	0.023	0.009	0.062	0.005	0.004	0.000	0.008	0.000	0.001	0.000	0.000	0.001	0.005
Zn	0.000	0.000	0.000	0.000	0.002	0.003	0.001	0.000	0.000	0.00	0.000	0.000	0.003	0.001	0.000	0.018	0.017	0.000	0.000	-	0.000	0.000	0.000
Mg	0.959	1.098	1.408	1.531	1.284	0.910	0.707	0.833	0.593	1.478	1.802	1.543	0.360	2.935	2.963	0.600	0.469	0.000	0.001	0.000	0.001	1.875	5.086
Ca	0.021	0.037	0.002	0.003	0.000	0.016	0.898	0.898	0.884	0.024	0.083	0.032	0.609	0.000	0.003	0.000	0.000	0.457	0.485	0.128	0.361	1.879	0.000
Na	0.000	0.000	0.000	0.001	0.000	0.003	0.036	0.042	0.042	0.000	0.000	0.000	0.000	0.007	0.000	0.00	-	0.528	0.526	0.840	0.576	0.42	0.08
K	0.000	0.003	0.000	0.000	0.000	0.003	0.000	0.000	0.002	0.000	0.000	0.000	0.000	0.000	0.000	0.000	0.000	0.013	0.017	0.022	0.016	0.424	1.912
Total	4.005	3.992	4.011	3.980	3.984	3.998	4.018	4.002	4.012	8.000	7.998	7.967	8.008	14.001	14.018	3.021	2.993	4.996	5.021	4.984	4.961	15.745	15.870
XMg	0.49	0.58	0.79	0.82	0.73	0.47	0.69	0.88	0.58	0.49	0.63	0.53	0.15	0.77	0.83	0.57	0.49					0.44	0.91
almandine										0.50	0.36	0.46	0.66										
pyrope										0.49	0.60	0.52	0.12										
grossular										0.01	0.03	0.01	0.20										
spessartine										0.00	0.01	0.00	0.02										

* total Fe as FeO

Sample No.	Rock name
A90021702B	Orthopyroxene-bearing felsic gneiss (Gof)
A90021603D	Garnet-bearing felsic gneiss (Ggf)
B98012802D	Mafic granulite (Gm)
A900217GA	Garnet-orthopyroxene granulite (Ggo)
C98012802	Ultramafic granulite (Gu)
A98012902D	Sapphirine-garnet-orthopyroxene gneiss (Gsa)
A98013107A	Corundum-spinel-sapphirine-phlogopite gneiss (Gsa)
B98021108A	Garnet-two pyroxene metamorphosed dyke gneiss (Dm)

Analyticdal data are after Tsunogae *et al* . (1999), Hokada *et al* . (1999) and Osanai (unpublished data).

gneous rock and komatiitic ultramafic igneous rock, respectively. In figure 5 these metamorphic rocks show well-defined correlation line and it may be indicating a differentiation trend during their emplacement stage of Archaean age.

The mafic gneisses and the ultramafic rocks range from 42 to 55 wt % in SiO_2. Some of these rocks are characterized by high MgO (up to 31 wt %), Cr (up to 5400 ppm) and Ni (up to 1800 ppm) contents. In the diagram of atomic (Fe_{total} + Ti) – Al - Mg showing calc-alkaline, tholeiitic and komatiitic fields after Jensen (1976), the mafic gneisses and ultramafic rocks plot within the range from komatiite to tholeiitic basalt field through komatiitic basalt (Fig. 6). Chondrite normalized REE patterns of the mafic gneisses and the ultramafic rocks are divided into two, 1) enrichment in LREE and slight depletion in HREE and 2) almost flat pattern. The REE pattern of the deformed sample, however, is a convex upward. This pattern may be influenced by later tectonic event since this sample has undergone mylonitic deformation. The REE pattern combined with major and trace elements of the mafic gneisses and the ultramafic rocks from Tonagh Island excluding the deformed sample suggest that protolith of these rocks had similar petrochemical character to komatiite and komatiitic basalt from Archaean greenstone belt.

Sapphirine-bearing granulites and gneisses have various chemical compositions from 38 to 78 wt% in SiO_2. The sapphirine-bearing granulites and gneisses could be derived from three different types of their origin such as 1) metasomatic origin between ultramafic rock and felsic gneiss, 2) restitic nature remaining after partial melting of surrounding rocks, and 3) originally magnesian- and aluminous quartz dominant rock as described above (chapter 3.10). These three different types show characteristically different chemical compositions in each other (Fig. 7). Types-1 and -2 sapphirine granulites have lower SiO_2 content while Al_2O_3 content in type-1 is slightly lower than type-2. On the other hand, type-3 has high in SiO_2. Other sapphirine-bearing garnulites and gneisses are also plot in these three areas (Fig. 7).

Bulk chemical compositions of the alkali-dolerite dikes and the metamorphosed mafic dikes are given in Table 4. The SiO_2 contents of the alkali-dolerite dikes range from 48 to 49 wt %. Chemical compositions among the measured samples are similar regardless of the grain sizes of samples and widths of intrusions. These dolerite dikes are characterized by high Na_2O/K_2O (2.24 to 2.43) ratios and high TiO_2 (2.07 to 2.16 wt %) contents. MORB normalized trace element concentrations of the alkali-dolerite dikes resemble those of the within-plate basaltic rocks. The normalized abundance of the metamorphosed dikes are higher in Zr and Y and lower in Sr, Nb and P than those of the alkali-dolerite although the pattern is similar to those of the alkali-dolerite.

8. Geophysics

Several kind of geophysical and geodetic observations were carried out along with JARE-39 at Tonagh Island. Five geophysical reference points were established by the Geographical Survey Institute (GSI) to connect with the other important reference points around the Enderby Land Region, such as those at Syowa Station (69.0°S, 39.5°E). Three reference points were set in the northern part, on the contrary, the rest two were set in the southern part of Tonagh Island (Fig. 8). At first, a precise coordinate was determined in WGS84 geodetic system for the site GSI 39-08 by conducting relative

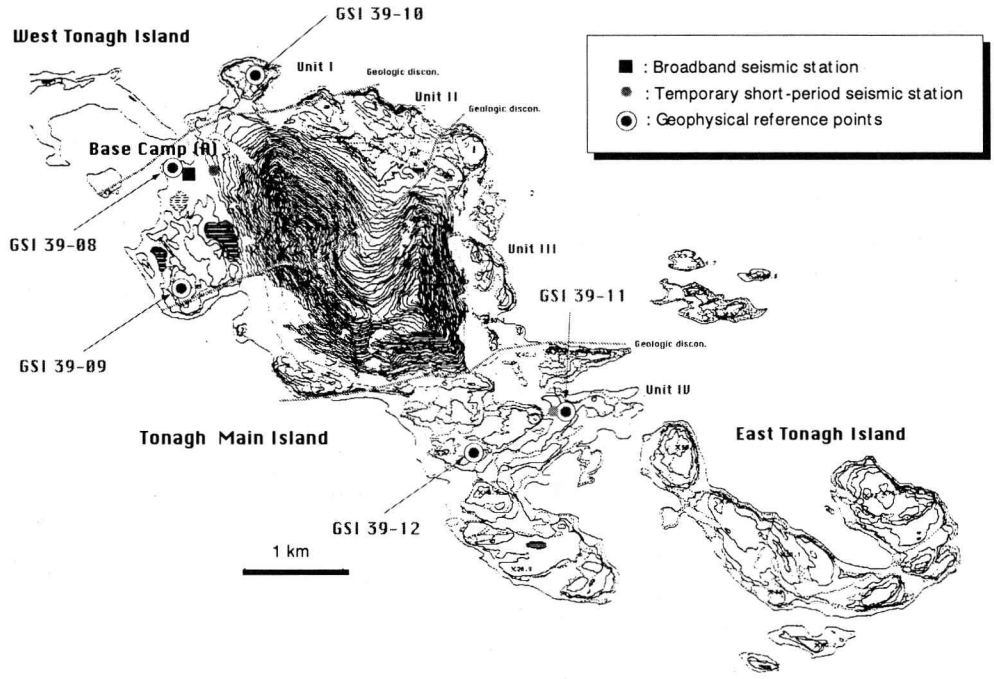

Fig. 8 Map showing the location of five geophysical reference points (double circles with solid inside) and seismic stations (solid square; broadband, solid circle; temporary short-period) at Tonagh Main Island.

positioning for Global Positioning System (GPS) with the Scientific Committee on Antarctic Research (SCAR)-GPS point (No. 23-16 Marker) at Syowa Station. Then coordinates of the other four reference points were obtained by making another relative positioning with the site GSI 39-08 (Table 6).

Gravity measurements at the four reference points at Tonagh Island were also conducted during JARE-39 fieldwork by land-type gravity meters. The determined free-air and Bouguer anomaries by a LaCoste-Romberg gravity meter (G-515) are listed in Table 6 (after Kanao and Higashi, 1999). The obtained values by a Scintrex gravity meter (CG-3) also indicate the same features for gravity values. The absolute gravity value at IAGBN-A reference point at Syowa Station (g=982524.327 mGal; Yamamoto, 1996) was referred to make a gravity anomaly calculation for each measurement point. Bouguer anomaries obtained at Tonagh Main Island indicate higher values about 30 mGal comparing to those at Syowa Station: That indicates an existence of thinner crustal depth around the Amundsen Bay Region than around the Lützow-Holm Bay.

Additionally, testing measurements to detect land-ocean ground noises were conducted by short-period (2Hz) seismometers and 16 bit A/D data loggers near the Base Camp (A) (20 February, 1998) (position should be refer to Osanai *et al.*, 1999) and near the reference point of GSI 39-11 (22 February, 1998) with observation time about six hours for each measurement point. The preliminary data in order to evaluate the ground noise condition were obtained in these short-term periods of observations. At present in

Table 6 WGS84 coordinates by relative GPS positioning and gravity anomaries by G-515 LaCoste-Romberg gravity meter for five reference points at Tonagh Main Island.

STATION NAME	LATITUDE degree	LONGITUDE degree	HEIGHT meter	GRAVITY mGal	FREE-AIR mGal	BOUGUER mGal
GSI 39-08	- 67.0878611111	50.2568377222	49.97200	982444.497	20.65	19.17
GSI 39-09	- 67.0993757778	50.2565723056	82.67700	982436.525	22.01	16.87
GSI 39-10	- 67.0799551389	50.2776931111	89.84000	982425.429	10.09	5.72
GSI 39-11	- 67.1121413333	50.3595535278	48.19600	982438.854	12.94	11.66
GSI 39-12	- 67.1219759444	50.3347302222	80.77500	982438.854	12.94	11.66

JARE-41 summer season, a broad-band seismometer (CMG-40T) with 16 bit A/D data recorder have been operated near the Base Camp (A) for about two months during February-March in 1999. A subsurface crustal structure will be obtained by analyzing the obtained data by this seismometer. Sharp seismic velocity discontinuities in the upper mantle are reported in the Archearn regions by tomographic models (Polet and Anderson, 1995). These seismic boundaries could be identified such as by large amplitudes of later phases for teleseismic receiver functions. In similar with the other Archearn cratons, thick lithospheric mantle would exist benearth the central Napier Complex area.

References

Asami, M., Suzuki, K., Grew, E.S. and Adachi, M. (1998): CHIME ages for granulites from the Napier Complex, East Antarctica. Polar Geosci., **11**, 172-199.

Audibert, N., Bertrand, P., Hensen, B.J., Kienast, J.R. and Ouzegane, K. (1993): Cordierite-K-feldspar-quartz-orthopyroxene symplectite from southern Algeria: new evidence for osumilite in high-grade metamorphic rocks. Mineral. Mag., **57**, 354-357.

Berg, J.H. and Wheeler, E.P. (1976): Osumilite of deep-seated origin in the contact aureole of the anorthositic Nain Complex, Labrador. Amer. Minaral., **61**, 29-37.

Black, L. P. (1988): Isotopic resetting of U-Pb zircon and Rb-Sr and Sm-Nd whole-rock systems in Enderby Land, Antarctica: Implication for the interpretation of isotopic data from polymetamorphic and multiply deformed terrains. Precambrian Res., **38**, 355-365.

Black, L.P., James, P.R. and Harley, S.L. (1983): The geochronology, structure and metamorphism of early Archaean rocks at Fyfe Hills, Enderby Land, Antarctica. Precanbrian Res., **21**, 197-222.

Black, L.P., Williams, I.S. and Compston, W. (1986a): Four zircon ages from one rock: the history of a 3930 Ma-old granulite from Mount Sones, Enderby Land, Antarctica. Contrib. Mineral. Petrol., **94**, 427-437.

Black, L.P., Sheraton, J.W. and James, P.R. (1986b): Late Archaean granulites of the Napier Complex, Enderby Land, Antarctica: a comparison of Rb-Sr, Sm-Nd, and U-Pb isotopic systematics in a complex terrain. Precamb. Res., **32**, 343-368.

Crohn, P.W. (1959): A contribution to the geology and glaciology of the western part of Australian Antarctic Territory. Bureau of Mineral Resources, Australia, Bull., 52.

Dallwitz, W.B. (1968): Co-existing sapphirine and quartz in granulite from Enderby Land, Antarctica. Nature, **219**, 476-477.

DePaolo, D.J., Manton, W.I., Grew, E.S and Halpern, M. (1982): Sm-Nd, Rb-Sr, and U-Th-Pb systematics of granulite-facies rocks from Fyfe Hils, Enderby Land, Antarctica. Nature, **298**, 614-618.

Ellis, D.J. (1980): Osumilite-sapphirine-quartz granulites from Enderby Land, Antarctica: P-T conditions of metamorphism, implications for garnet-cordierite equilibria and the evolution of the deep crust. Contrib. Mineral. Petrol., **74**, 201-210.

Grew, E.S. (1980): Sapphirine + quartz association from Archaean rocks in Enderby Land, Antarctica. Amer. Mineral., **65**, 821-836.

Grew, E.S. (1982): Osumilite in the sapphirine-quartz terrane of Enderby Land, Antarctica: implications for osumilite petrogenesis in the granulite facies. Amer. Mineral., **67**, 762-787.

Grew, E.S. and Manton, W.I. (1979): Archean rocks in Antarctica: 2.5 billion-year uranium-lead ages of pegmatites in Enderby Land, Antarctica. Science, **206**, 443-445.

Griffin, A.C. (1979): Structural evolution of Archaean supracrustal rocks at Amundsen Bay, East Antarctica (Abstract). Jour Geol Soc. Australia, **26**, 271.

Grikurov, G.E., Znachko-Yavorsky, G.A., Lamenev, E.N and Ravich, M.G. (1976): Explanatory notes to the geological map of Antarctica (Scale 1:5,000,000). Res. Inst. Arctic Geol., USSR Ministry of Geol., Leningrad.

Harley, S.L. (1985): Garnet-orthopyroxene bearing granulites from Enderby Land, Antarctica: metamorphic pressure-temperature-time evolution of the Archaean Napier Complex. Jour. Petrol., **26**, 819-856.

Harley, S. L. (1987): A pyroxene-bearing meta-ironstone and other pyroxene-granulites from Tonagh Island, Enderby Land, Antarctica: further evidence for very high temperature (>980°C) Archaean regional metamorphism in the Napier Complex. J. Metamorphic Geol., **5**, 341-356.

Harley, S.L. (1998): On the occurrence and characterization of ultrahigh-temperature crustal metamorphism. In Treloar, P.J. and O'Brien, P.J. eds., What drives metamorphism and metamorphic reactions?, Geol. Soc. London Spec. Publ., **138**, 81-107.

Harley, S.L. and Black, L.P. (1997): A revised Archaean chronology for the Napier Complex, Enderby Land, from SHRIMP ion-microprobe studies. Antarct. Sci., **9**, 74-91.

Harley, S. L. and Hensen, B. J. (1990): Archaean and Proterozoic high-grade terranes of East Antarctica. (40-80°E): A case study of diversity in granulite facies metamorphism. High-temperature Metamorphism and Crustal Anatexis. ed. by J. R. Ashworth and M. Brown. London, Unwin Hyman, 320-370 (Mineral. Soc. Ser., 2).

Hokada, T. (1999): Thermal evolution of the Ultrahigh-temperature metamorphic rocks in the Archaean Napier Complex, East Antarctica. Ph.D. Thesis of the Graduate University for Advanced Studies.

Hokada, T., Osanai, Y., Toyoshima, T., Owada, M., Tsunogae, T. and Crowe, W.A. (1999): Petrology and metamorphism of sapphirine-bearing aluminous gneisses from Tonagh Island in the Napier Complex, East Antarctica. Polar Geosci., **12**, 49-70.

Ishikawa, M., Motoyoshi, Y. and Fraser, G.L. (1994): Preliminary report of structure of Forefinger Point, Enderby Land, East Antarctica. Proc. NIPR Symp. Antarct. Geosci., **7**, 90-100.

Ishikawa, M. Hokada, T., Ishizuka, H., Miura, H., Suzuki, S., Takada, M. and Zwartz, D.P. (2000): Geological map of Mount Riiser-Larsen, Enderby Land, Antarctica. Antarct. Geol. Map. Ser., Sheet 37 (with explanatory text 23p). Tokyo, Natl Inst. Polar Res.

Ishizuka, H., Ishikawa, M., Hokada, T. and Suzuki, S. (1998): Geology of the Mt. Riiser-Larsen area of the Napier Complex, East Antarctica. Polar Geosci., **11**, 154-171.

Ishizuka, H. and Suzuki, S. (1999): Diversity and origins of the Amundsen Dikes, part 1: bulk rocks and mineral compositions. Abstract of the 19th Symposium on Antarctic Geosciences, National Institute of Polar Research, 70.

James, P. R. and Black, L. P. (1981): A review of the structural evolution and geochronology of the Archaean Napier Complex of Enderby Land, Australian Antarctic Territory. Archaean Geology: Second International Symposium. Perth, 1980, ed. by J. E. Glover and D. I. Groves. Sydney, Geol. Soc. Aust., 71-83 (Spec. Publ. Geol. Soc. Aust., 7).

Jensen, L.S. (1976): A new cation plot for classifying subalkalic volcanic rocks. Ontario Div. Mines. Misc. Pap. 66.

Kamenev, E.N. (1972): Geological structure of Enderby Land. Antarctic geology and geophysics, ed. By R.J. Adie. Oslo, Universitetsforlaget, 579-583.

Kamenev, E.N. (1975): The geology of Enderby Land. Acad Sci. USSR Comm. Antarct. Res. Rept., 14.

Kanao, M. and Higashi, T. (1999): Geophysical research from field observations by the Earth Science Division in the 38th Japanese Antarctic Research Expedition (1996-1998), *Antarct. Rec.*, **43**, 375-405.

Makimoto, H., Asami, M. and Grew, E.S. (1989): Some geological observations on the Archean Napier Complex at Mount Riiser-Larsen, Amundsen Bay, Enderby Land. Proc. NIPR Symp. Antarct. Geosci., **3**, 128-141.

Mawson, D. (1932): The B.A.N.Z. Antarctic Research Expedition 1929-1931. Geographycal Jour., **80**, 101-113.

McCulloch, M.T. and Black, L.P. (1984): Sm-Nd isotopic systematics of Enderby Land granulites and evidence for the redistribution of Sm and Nd during metamorphism. Earth Planet. Sci. Lett., **71**, 46-58.

McLeod, I.R. (1959): Report on geological and glaciological work by the 1958 Australian Nationa Antarctic Research Expedition. Bureau of Mineral and Resources, Australia, Record 1959/131.

McLeod, I.R. (1964): An outline of geology of the sector from longitude 45° to 80°E, Antarctica. Antarctic Geology, ed. By R.J. Adie. Amsterdam, North-Holland Publ. Co. 237-247.

McLeod, I.R., Trail, D.S., Cook, P.J. and Wallis, G.R. (1966): Geological work in Antarctica, January to March, 1965. Bureau of Mineral and Resources, Australia, Record 1966/9.

Miyamoto, T., Grew, E.S., Sheraton, J.W., Yates, M.G., Dunkley, D.J., Carson, C.J. Yoshimura, Y. and Motoyoshi, Y. (2000): Lamproite dykes in the Napier Complex at Tonagh Island, Enderby Land, East Antarctica. Polar Geosci., **13**, 41-59.

Motoyoshi, Y. (1998): Ultra-high temperature metamorphism of the Napier Complex, East Antarctica: a metamorphic perspective. Jour. Geol. Soc. Japan, **104**, 794-807 (in Japanese with English abstract).

Motoyoshi, Y., Ishikawa, M. and Fraser, G.L. (1994): Reaction textures in granulites from Forefinger Point, Enderby Land, Antarctica: an alternative interpretation on the metamorphic evolution of the Rayner Complex. Proc. NIPR Symp. Antarct. Geosci., **7**, 101-114.

Motoyoshi, Y., Ishikawa, M. and Fraser, G.L. (1995): Sapphirine-bearing silica-undersaturated granulites from Forefinger Point, Enderby Land, Antarctica: evidence for a clockwise P-T path? Proc. NIPR Symp. Antarct. Geosci., **8**, 121-129.

Motoyoshi, Y. and Hensen, B.J. (1989): Sapphirine-quartz-orthopyroxene symplectites after cordierite in the Archaean Napier Complex, Antarctica: Evidence for a counterclockwise P-T path? Eur. Jour. Mineral., **1**, 467-471.

Motoyoshi, Y., Hensen, B.J. and Matsueda, H. (1990): Metastable growth of corundum adjacent to quartz in a spinel-bearing quartzite from the Archaean Napier Complex, Antarctica. Jour. Metamorphic Geol., **8**, 125-130.

Motoyoshi, Y. and Matsueda, H. (1984): Archean granulites from Mt. Riiser-Larsen in Enderby Land, East Antarctica. Mem. Natl. Inst. Polar Res., Spec. Issue, **33**, 103-125.

Motoyoshi, Y., Miura, H., Yamauchi, H., Yoshimura, Y., Miyamoto, T., Yoshinaga, S., Ohashi, Y., Maki, K., Harigai, S., Takei, T., Grew, E.S., Carson, C.J. and Dunkley, D.J. (1999): Report on the geological and geomorphological field operation in the Amundsen Bay region, wester Enderby Land, 1998-1999 (JARE-40). Nankyoku Shiryô (Antarctic Record), **43**, 534-570.

Osanai, Y., Owada, M., Shiraishi, K., Hensen, B.J. and Tsuchiya, N. (1995): Metamorphic evolution of deep crustal high-temperature granulites from Tonagh Island in the Archaean Napier Complex, East Antarctica. Abst. VII Intl. Symp. Antarct. Earth Sci., Siena (Italy), 289.

Osanai, Y., Toyoshima, T., Owada, M., Tsunogae, T., Hokada, T. and Crowe, W. A., (1999): Geology of ultrahigh-temperature metamorphic rocks from Tonagh Island in the Napier Complex, East Antarctica. Polar Geosci., **12**, 1-28.

Owada, M., Osanai, Y. and Kagami, H. (1994): Isotopic equilibration age of Sm-Nd whole-rock system in the Napier Complex (Tonagh Island), East Antarctica. Proc. NIPE Symp. Antarct. Geosci., **7**, 122-132.

Owada, M., Osanai, Y., Toyoshima, T., Tsunogae, T., Hokada, T. and Crowe, W.A. (1999): Petrography and geochemistry of mafic and ultramafic rocks from Tonagh Island in the Napier Complex, East Antarctica: a preliminary report. Polar Geosci., **12**, 87-100.

Owada, M., Osani, Y., Tsunogae, T., Toyoshima, T., Hokada, T. and Crowe, W.A. (2000): LREE-enriched mafic gneiss and meta-ultramafic rock from Tonagh Island in the Napier Complex, East Antarctica. Polar Geosci., **13**, 86-102.

Polet, J. and Anderson, D.L. (1995): Depth extent of cratons as inferred from tomographic studies, *Geology*, **23**, 205-208.

Rucker, R.A. (1963): Geological reconnaissance in Enderby Land and southern Prince Ckarles Mountains, Antarctica. Bureau of Mineral and Resources, Australia, Record 1963/154.

Sandiford, M.A. (1985): The metamorphic evolution of granulites at Fyfe Hills: implications for Archaean crustal thickness in Enderby Land, Antarctica. Jour. Metamorphic Geol., **3**, 155-178.

Sandiford, M.A. and Wilson, C.J.L. (1983): The geology of the Fyfe Hills-Khamara Bay region, Enderby Land. eds. By R.L. Oliver, P.R. James and J.B. Jago. Antarctic Science. Australian Acad, Sci., Canberra, 16-19.

Sandiford, M.A. and Wilson, C.J.L. (1984): The structural evolution of the Fyfe Hills-Khamara Bay region, Enderby Land, East Antarctica. Australian Jour Earth Sci., **31**, 403-426.

Sandiford, M.A. and Wilson, C.J.L. (1986): The origin of Archaean gneisses in the Fyfe Hills region, Enderby Land: field occurrence, petrography and geochemistry. Precambrian Res., **31**, 37-68.

Sheraton, J.W. (1980): Geochemistry of Precambrian metapelites from East Antarctica: secular and metamorphic variations. BMR Jour. Australian Geology and Geophysics, 5, 279-288.

Sheraton, J.W. (1984): Chemical changes associated with high-grade metamorphism of mafic rocks in the East Antarctic Shield. Chemical Geol., **47**, 135-157.

Sheraton, J.W. (1985): Geology of Enderby Land and Western Kemp Land, Australian Antarctic Territory, Scale 1:500,000. Australian Bureau Miner. Resourc., Geology and Geophysics.

Sheraton, J.W., Offe, L.A., Tingey, R.J. and Ellis, D.J. (1980): Enderby Land, Antarctica- an unusual Precambrian high-grade metamorphic terrain. Jour. Geol. Soc. Australia, **27**, 1-18.

Sheraton, J.W. and Black, L.P. (1981): Geochemistry and geochronology of Proterozoic tholeiite dykes of East Antarctica: Evidence for mantle metasomatism. Contrib. Mineral. Petrol., **78**, 305-317.

Sheraton, J.W. and Black, L.P. (1983): Geochemistry of Precambrian gneisses: relevance for the evolution of the East Antarctic Shield. Lithos, **16**, 273-296.

Sheraton, J.W., Tingey, R.J., Black, L.P., Offe, L.A. and Ellis, D.J. (1987): Geology of Enderby Land and Western Kemp Land, Antarctica. Aust. Bur. Miner. Resourc. Bull., 223, 51p.

Shiraishi, K., Ellis, D.J., Fanning, C.M., Hiroi, Y., Kagami, H. and Motoyoshi, Y. (1997): Re-examination of the metamorphic and protolith ages of the Rayner Complex, Antarctica: evidence for the Cambrian (Pan-African) regional metamorphic event. In Ricci, C.A., ed., The Antarctic Region: Geological Evolution and Processes, Siena, Terra Antarctica Publication, 79-88.

Suzuki, S. (2000): Geochemistry and geochronology of ultra-high temperature metamorphic rocks from the Mt. Riiser-Larsen area in the Archaean Napier Complex, East Antarctica. Ph.D. Thesis of the Graduate University for Advanced Studies.

Suzuki, S., Hokada, T., Ishikawa, M. and Ishizuka, H. (1999): Geochemical study of granulites from Mount Riiser-Larsen, Enderby Land, East Antarctica: Implication for protoliths of the Archaean Napier Complex. Polar Geosci., **12**, 101-125.

Tainosho, Y., Kagami, H., Takahashi, Y., Iizumi, S., Osanai, Y. and Tsuchiya, N. (1994): Preliminary result for the Sm-Nd whole-rock age of the metamorphic rocks from Mount Pardoe in the Napier Complex, East Antarctica. Proc. NIPR Symp. Antarct. Geosci., **7**, 115-121.

Tainosho, Y., Kagami, H., Hamamoto, T. and Takahashi, Y. (1997): Preliminary result for the Nd and Sr isotope characteristics of the Archaean gneisses from Mount Pardoe, Napier Complex, East Antarctica. Proc. NIPR Symp. Antarct. Geosci., **10**, 92-101.

Toyoshima, T., Osanai, Y., Owada, M., Tsunogae, T., Hokada, T. and Crowe, W. A. (1999): Deformation of ultrahigh-temperature metamorphic rocks from Tonagh Island in the Napier Complex, East Antarctica. Polar Geosci., **12**, 29-48.

Tsunogae, T., Osanai, Y., Toyoshima, T., Owada, M., Hokada, T. and Crowe, W. A. (1999): Metamorphic reactions and preliminary P-T estimates of ultrahigh-temperature mafic granulite from Tonagh Island in the Napier Complex, East Antarctica. Polar Geosci., **12**, 71-86.

Warren, R.G. and Hensen, B.J. (1983): Scapolite-wollastonite-calcite assemblages in granulites from the Arunta Block and Antarctica. 6th Australian Geol. Convention, Canberra (abstract), 69-70.

Wellman, P. (1983): Interpretation of geophysical surveys –longitude 45° to 65°E, Antarctica. eds. By R.L. Oliver, P.R. James and J.B. Jago. Antarctic Science. Australian Acad, Sci., Canberra, 522-526.

Wellman, P. and Tingey, R.J. (1982): A garvity survey of Enderby and Kemp Lands, Antarctica. Ed. By C. Craddock. Antarctic Geoscience. University of Wisconsin Press, Madison, 937-940.

Williams, I.S., Compston, W., Black, L.P., Ireland, T.R. and Foster, J.J. (1984): Unsupported radiogenic Pb in zircon: a cause of anomalously high Pb-Pb, U-Pb and Th-Pb ages. Contrib. Mineral. Petrol., **88**, 322-327.

Yamamoto, H. (1996): Gravity measurements with the portable absolute gravimeter FG5 at Antarctica, *Bull. Geograph. Surv. Inst.,* **42**, 18-22.

Yoshimura, Y., Motoyoshi, Y., Grew, E.S., Miyamoto, T., Carson, C.J., and Dunkley, D.J. (2000): Ultrahigh-temperature metamorphic rocks from Howard Hills in the Napier Complex, East Antarctica. Polar Geosci., **13**, 60-85.

A

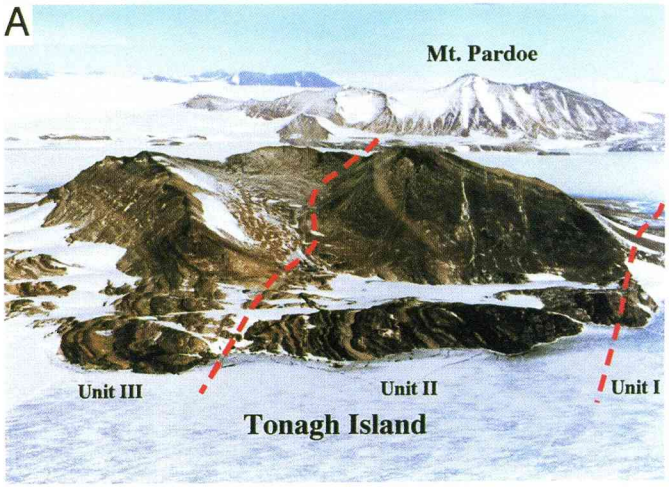

Plate 1. A: Northern part of Tonagh Island: viewed from helicopter. B: Layered structure composed mainly of orthopyroxene-bearing felsic gneiss, garnet-bearing felsic gneiss, two-pyroxene-bearing mafic granulite and garnet-orthopyroxene gneiss and granulite in the northern coast Viewed from northeast.

B

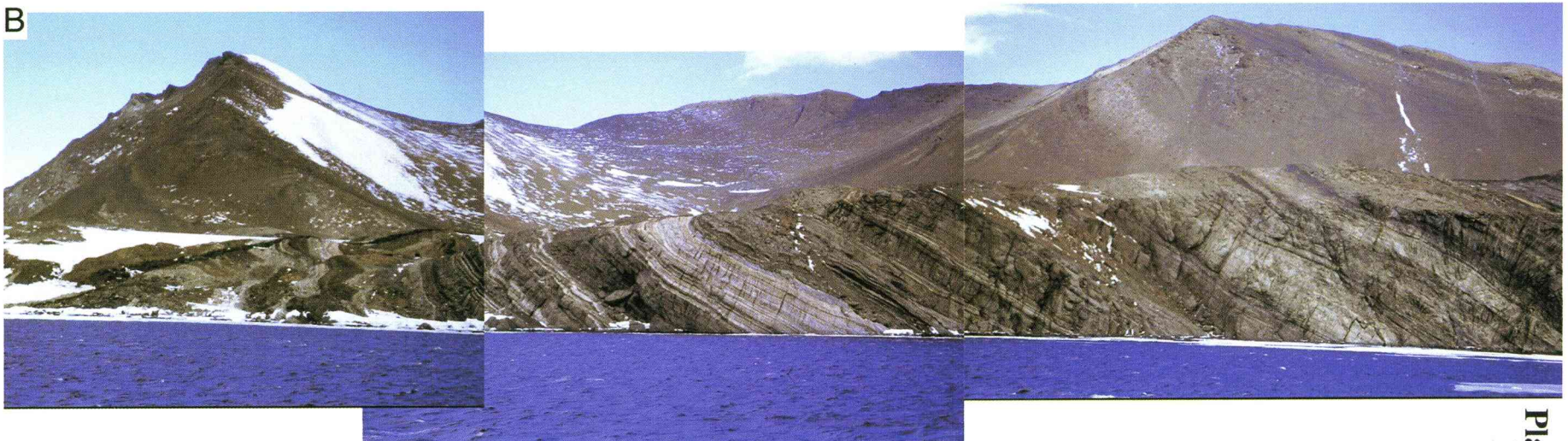

Plate 1

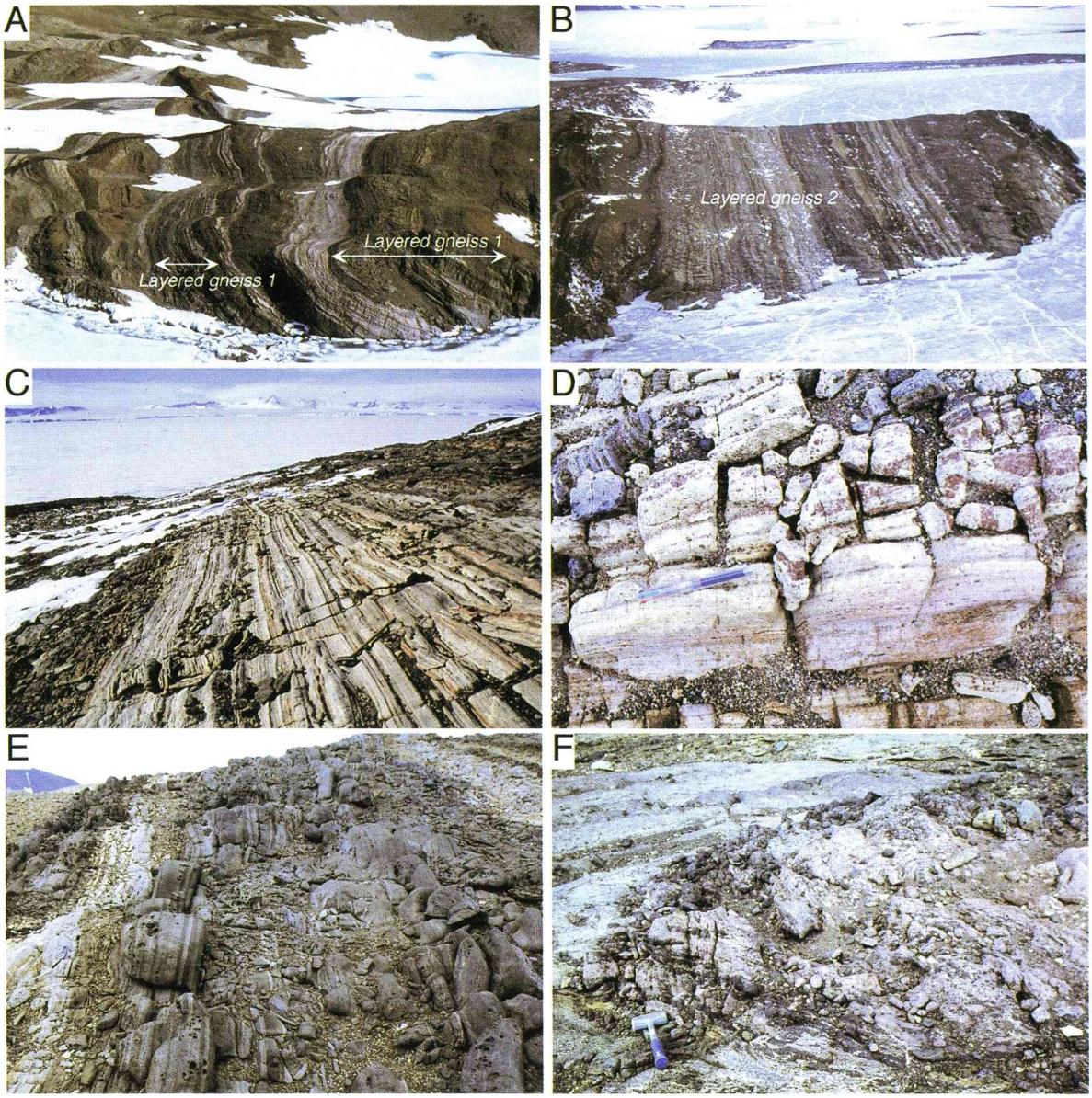

Plate 2. A: Layered gneiss 1 (alternation of dark brown and pale white layers) composed of felsic (mainly orthopyroxene-bearing) gneiss and two pyroxene-bearing mafic granulite. B: Thin alternation of the layered gneiss 2 in the northern peninsula. C: Thin layered-type orthopyroxene-bearing felsic gneiss. D: Layered-type garnet-bearing felsic gneiss with modal variation of garnet. E: Two pyroxene-bearing mafic granulite (dark layer) interlayered with orthopyroxene-bearing felsic gneiss (light grayish layer). F: Lenticular block of garnet-orthopyroxene granulite in the layered gneiss 2.

Plate 3

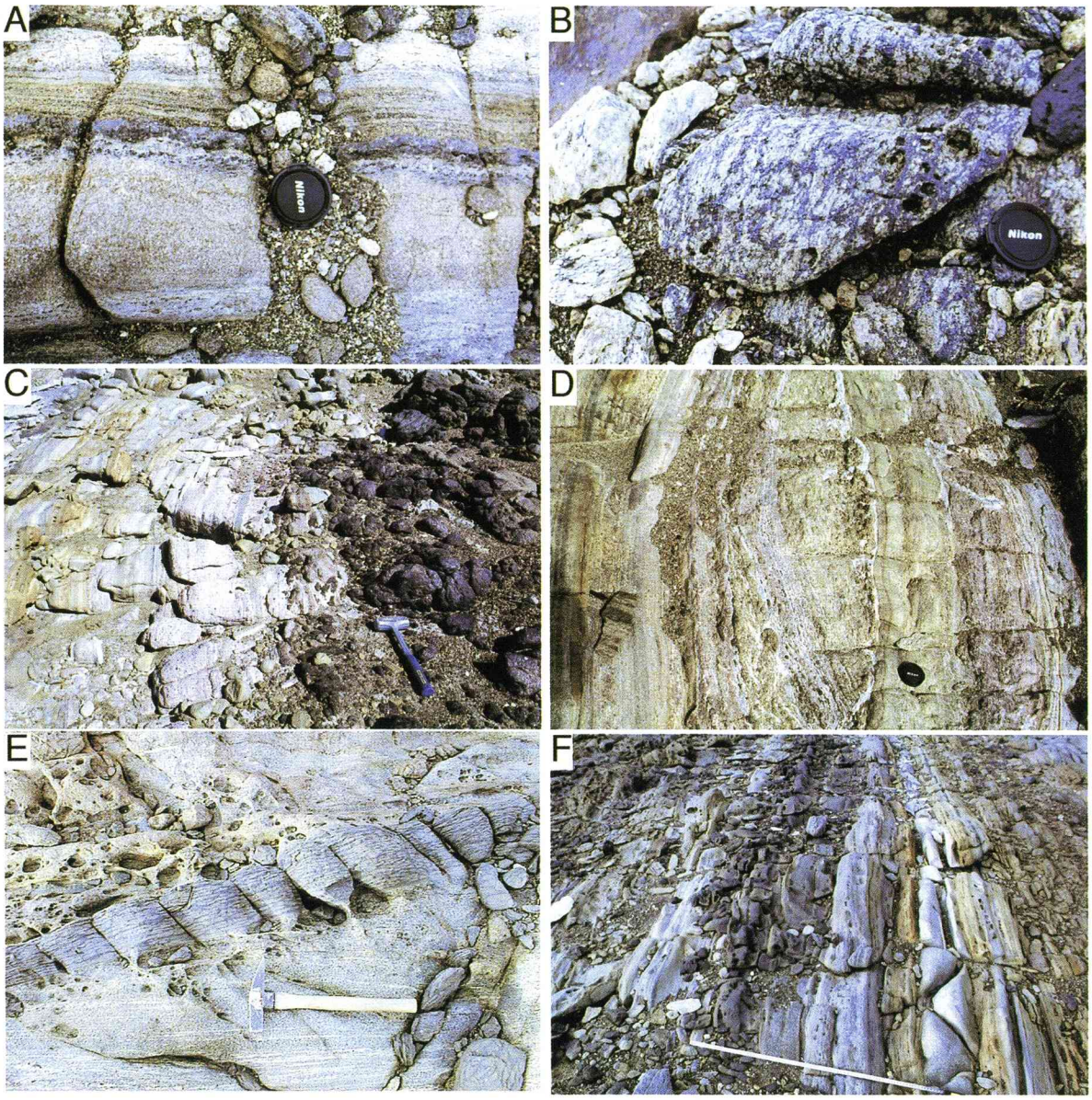

Plate 3. A: Garnet-orthopyroxene gneiss in the layered gneiss 2. B: Magnetite-quartz gneiss in the layered gneiss. C: Orthopyroxenite lenticular block (right-side dark colored part) in the orthopyroxene-bearing felsic gneiss (left-side pale grayish part). Note that the sapphirine-bearing aluminous gneiss (centered pinkish part) occurs as a reaction zone. D: Pale brownish-green lherzolitic block in layered gneiss with pinkish aluminous gneiss. E: Metamorphosed (garnet-two pyroxene) mafic dyke cutting the general foliation of surrounding orthopyroxene-bearing felsic gneiss along the shear zone at the boundary between Units II and III. F: Thin intercalations of impure quartzite (pale grayish layers) in the layered gneiss.

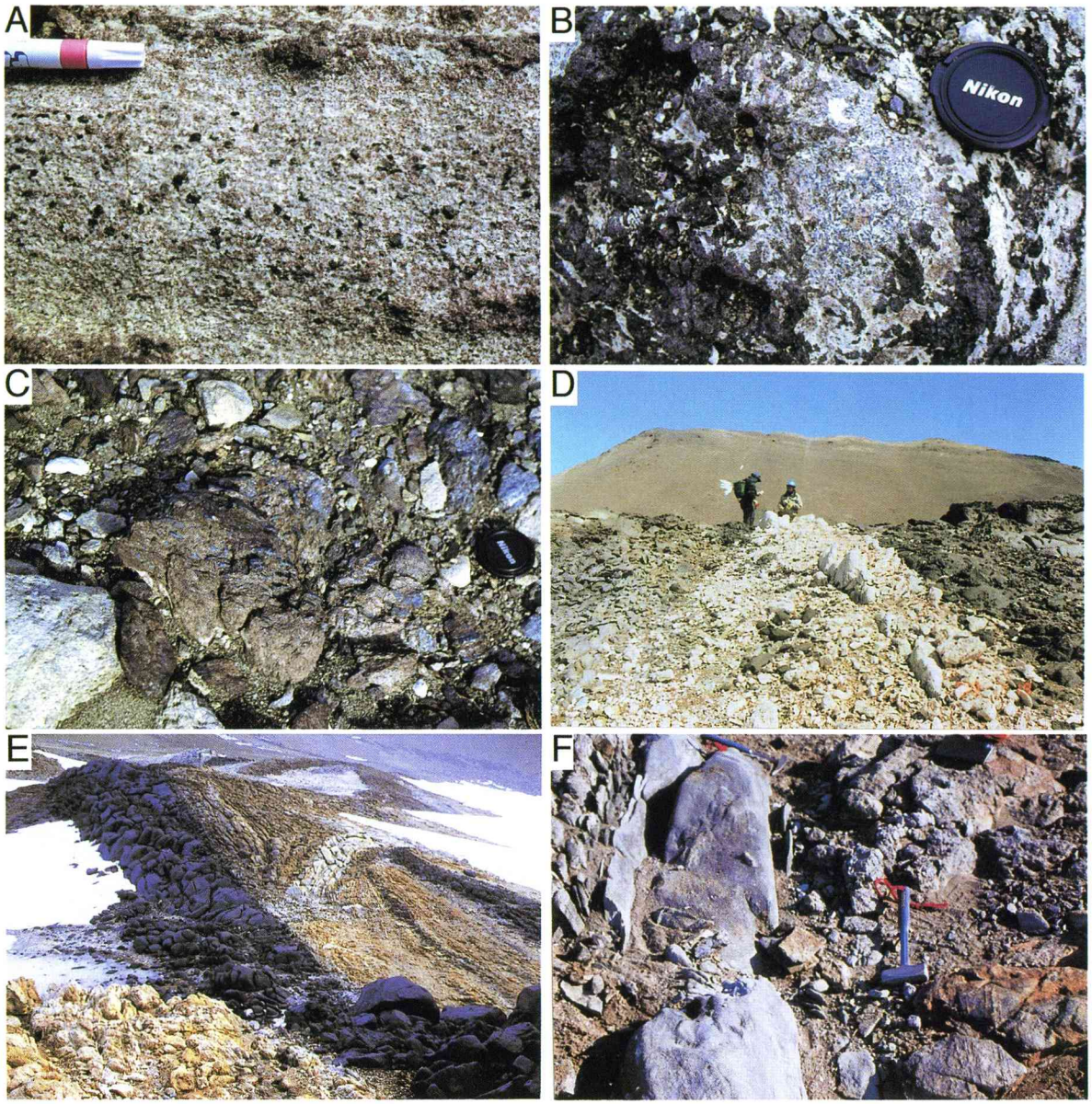

Plate 4. A: Sapphirine-garnet-orthopyroxene-cordierite-sillimanite granulite in the reaction zone between ultramafic and felsic gneisses. B: Sapphirine-orthopyroxene-garnet granulite block in the felsic gneiss. C: Sapphirine-spinel-corundum-phlogopite granulite in the felsic gneiss. D: Muscovite pegmatite from north part of Tonagh Island (Unit II). E: Unmetamorphosed mafic dyke (alkali-dolerite: Amundsen Dike), which cuts the host metamorphic foliations in Unit II obliquely. Width of dyke is c. 2 m. F: Lamproite dyke (left-side) in felsic gneiss (right-side) from southwest part of Tonagh Island.

Plate 5

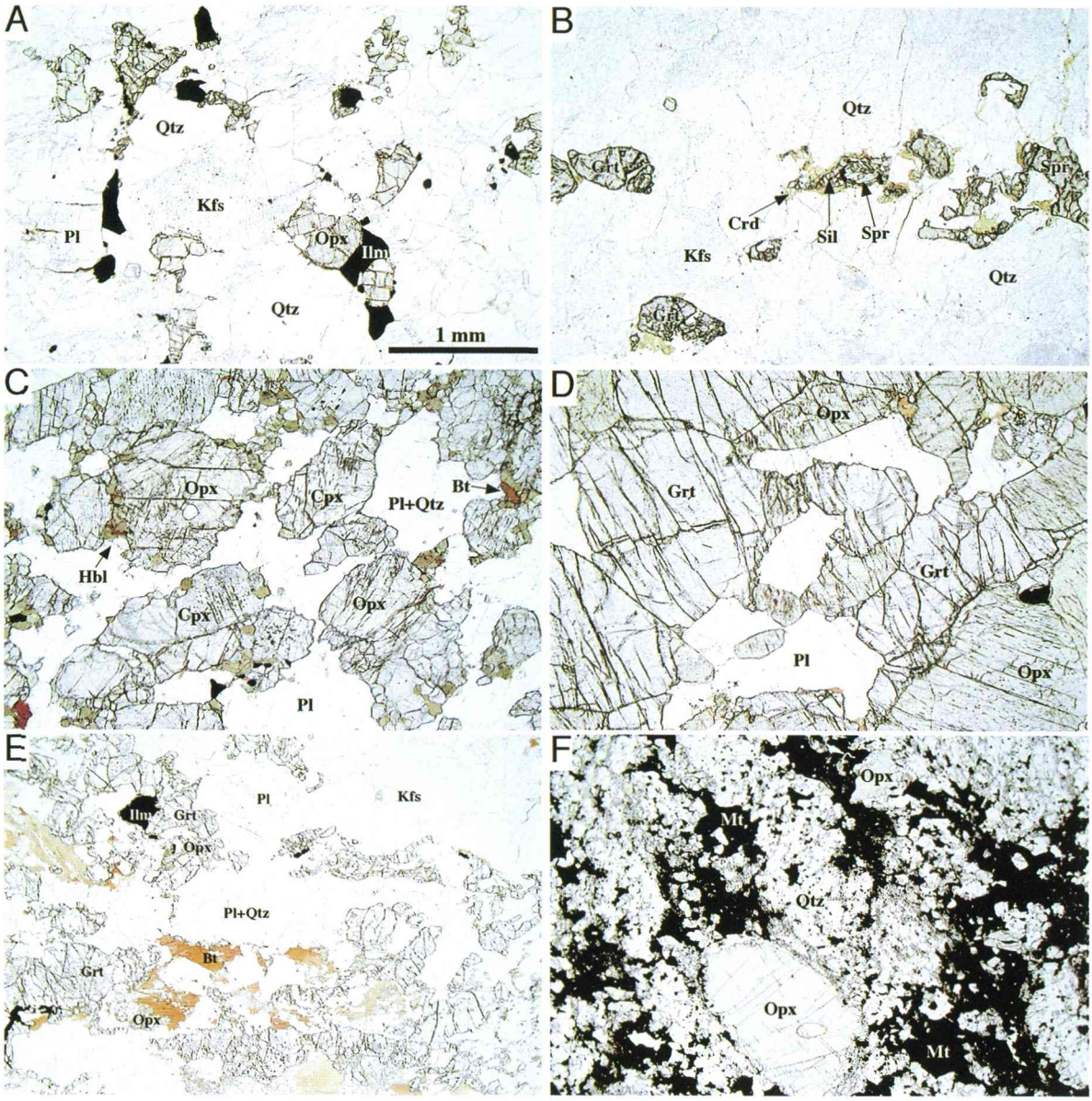

Plate 5. Photomicrograph of metamorphic rocks. Plane polarized light. Holizontal width of photograph is 3.6 mm. A: Typical orthopyroxene-bearing felsic gneiss. B: Garnet-bearing felsic gneiss containing sapphirine. Note that sapphirine and quartz are separated by a sillimanite and pinited cordierite most. C: Two pyroxene-bearing mafic granulite. Secondary hornblende and biotite are also present. D: Garnet-orthopyroxene granulite. Quartz and K-feldspar are also present. E: Fine-grained garnet-orthopyroxene gneiss with primary(?) biotite. F: Orthopyroxene-bearing magnetite-quartz gneiss (Mt: magnetite).

Plate 6

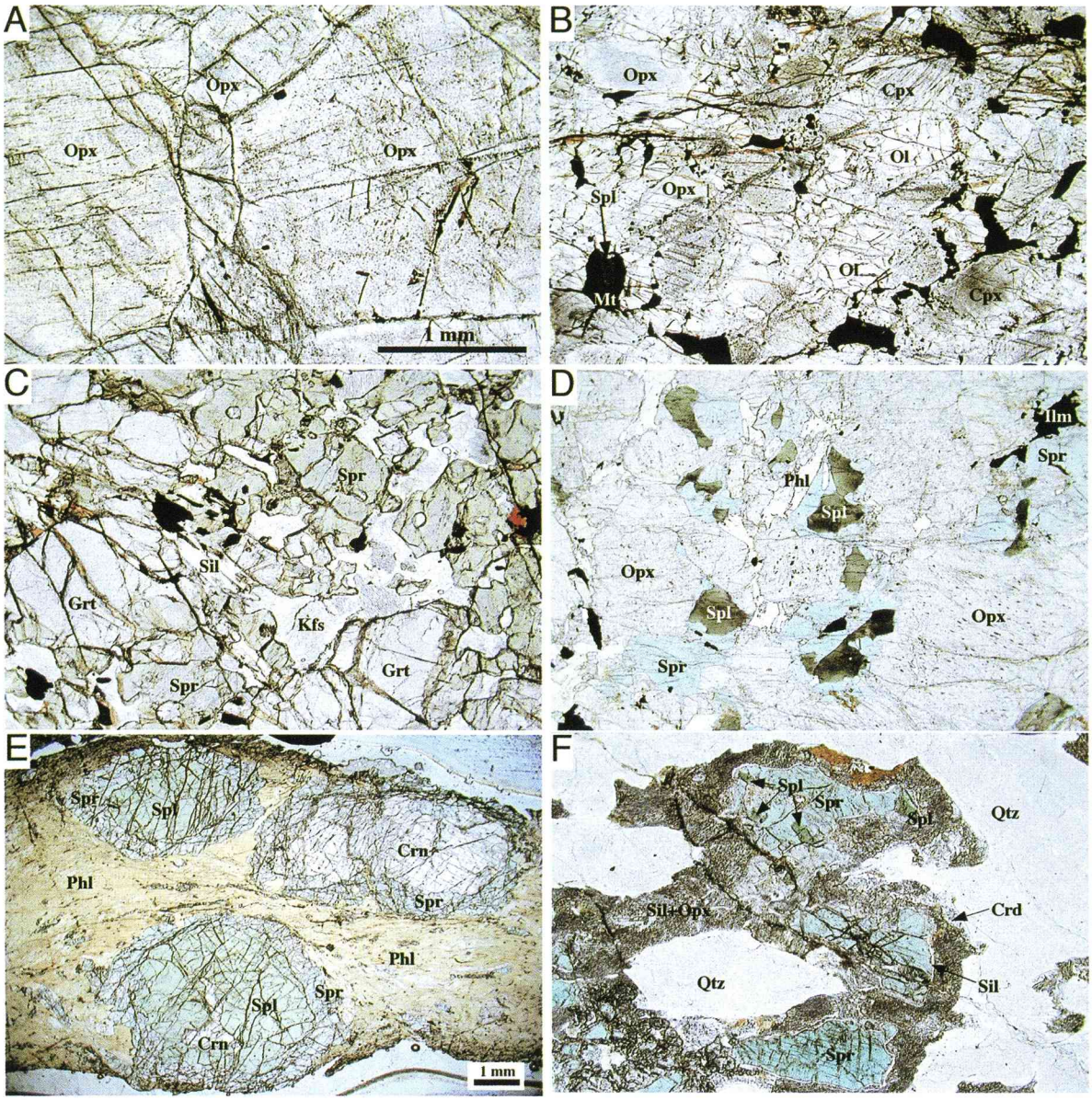

Plate 6. Photomicrograph of metamorphic rocks. Plane polarized light. Holizontal width of photograph is 3.6 mm (except Plate 6E). A: Orthopyroxenite. Note very fine grains of ilmenite needles in orthopyroxene. B: Metamorphosed lherzolitic ultramafic rock (Ol: olivine). C: Chromian green sapphirine-bearing aluminous granulite. Brownish chromian spinel is also present. D: Orthopyroxene-spinel-sapphirine-phlogopite granulite of lenticular block in the felsic gneiss. Note sapphirine occurs at the boundary between orthopyroxene and spinel. E: Sapphirine-spinel-corundum spots characteristically occur in the phlogopite-rich aluminous granulite as block in the felsic gneiss. F: Sapphirine-quartz granulite as a thin layer in layered gneiss. Note that the reaction product of orthopyroxene-sillimanite-cordierite symplectite occurs between sapphirine and quartz. Spl: spinel, Phl: phlogopite, Crn; corundum.

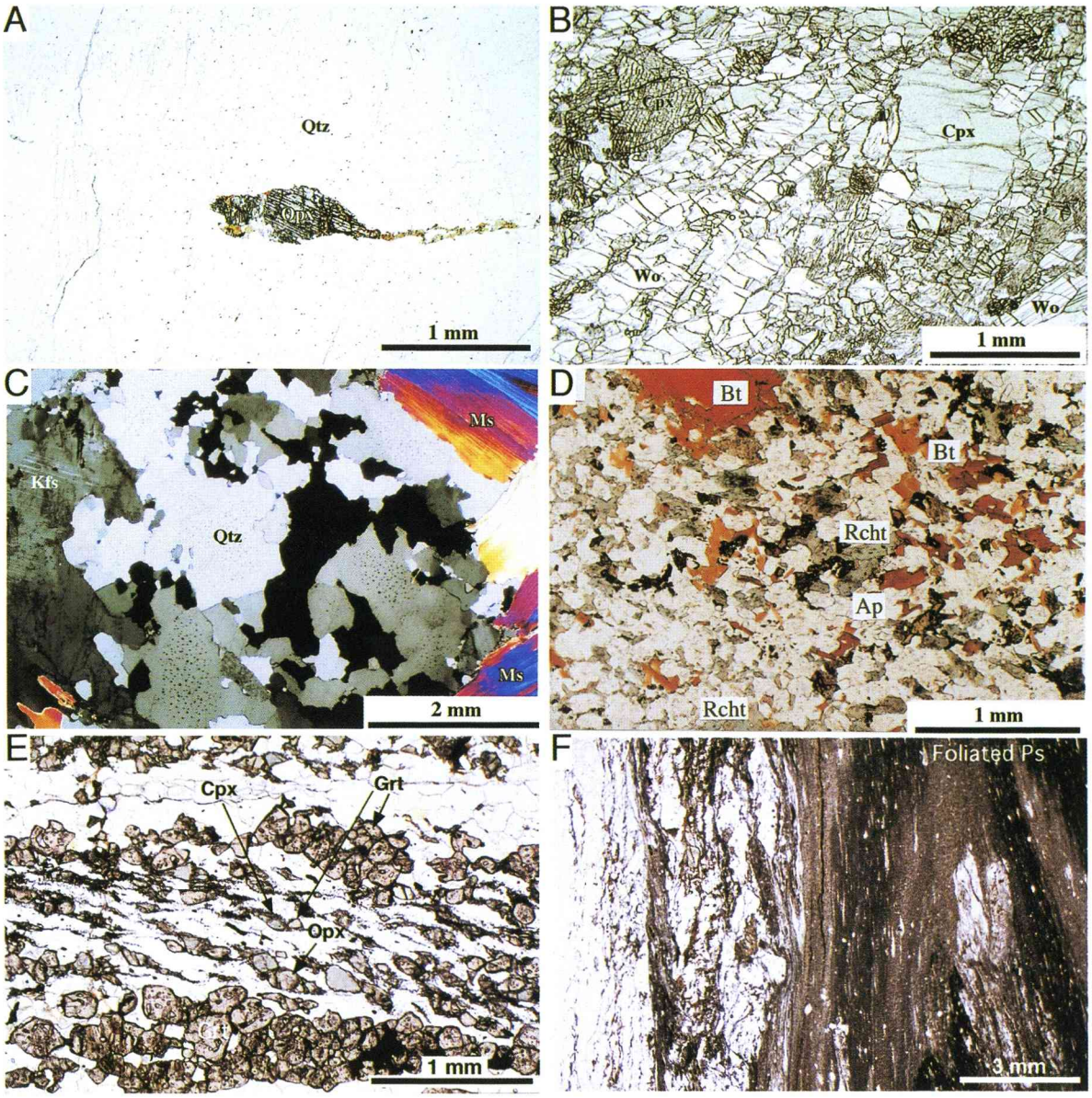

Plate 7. Photomicrograph of metamorphic rocks. Plane polarized light. A: Orthopyroxene-bearing quartzite with secondary biotite. B: Clinopyroxene-wollastonite-bearing calc-silicate gneiss. C: Muscovite pegmatite (TM990119-03A). Crossed polars. (Ms: muscovite) D: Biotite-bearing lamproite (TM990113-01A). (Ap: apatite, Rcht: richterite). E: D6 Orthopyroxene-Cpx-Grt mylonite formed along the western part of the boundary fault between units II and III. Alignment of the long axes of dynamically recrystallized fine grains of orthopyroxene (Opx), clinopyroxene (Cpx) and garnet (Grt) define oblique grain shape fabrics. Top-to-the-W (sinistral-normal) sense of shear. Plane-polarized light (PPL). (B98021504A) F: D6 foliated pseudotachylyte (Ps) in the D6 mylonite zone along the western part of the boundary fault between units II and III. The S6 foliation of the pseudotachylyte is continuous with and parallel to that of the surrounding D6 mylonite. PPL. (B98021505C)

Plate 8

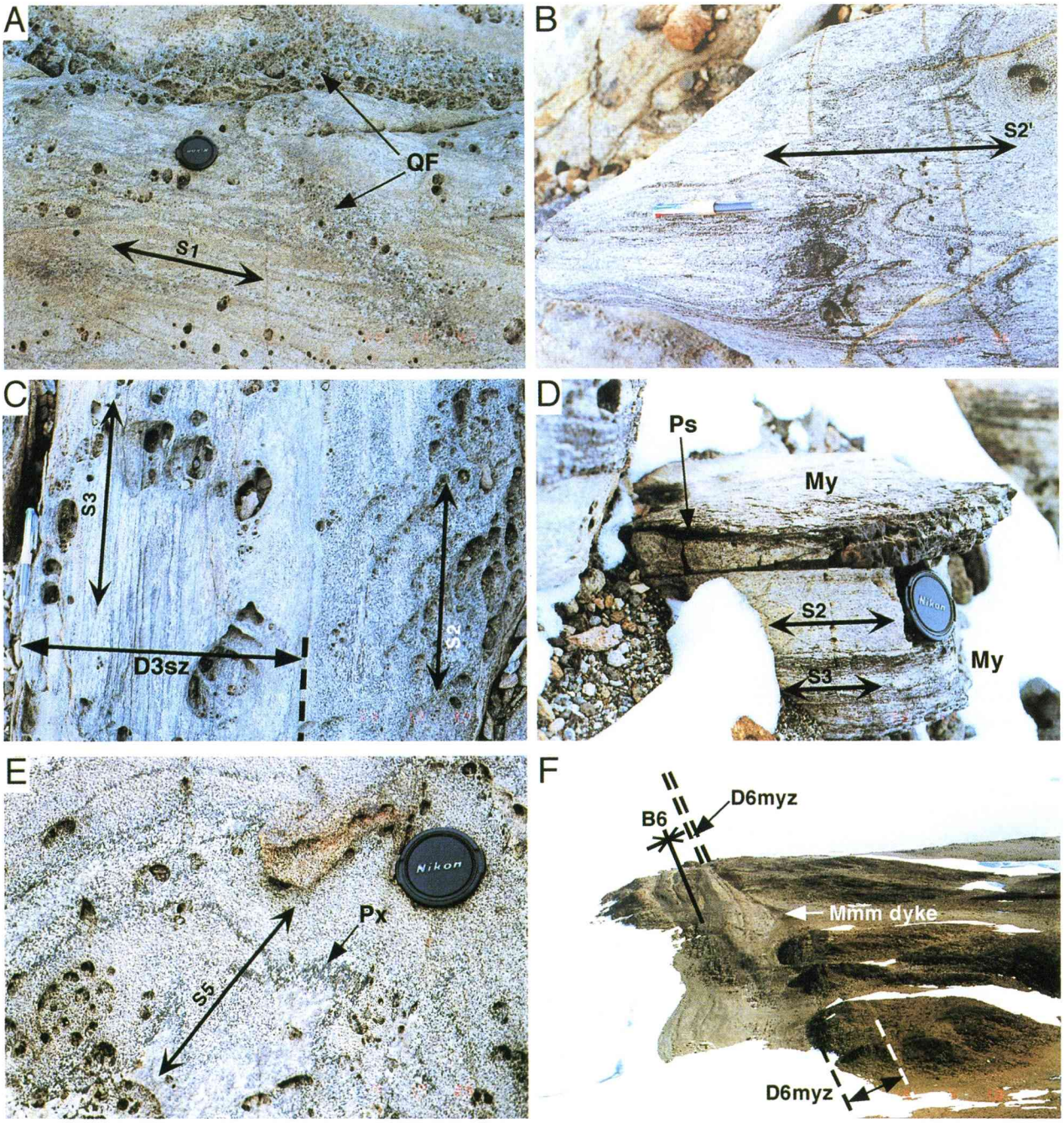

Plate 8. D1 to D6 deformation structures. A: D1 quartzo-feldspathic vein (QF) cutting across S1 foliation (S1) in the western part of unit II. S1 is parallel to lithological boundaries and compositional layering of sedimentary precursors of metamorphic rocks. B: B2 intrafolial fold with remarkable S2' axial foliation in orthopyroxene-bearing quartzofeldspathic gneiss from the western part of unit II. C: D3 mylonite zone (D3sz) parallel to S2 foliation (S2) in orthopyroxene-bearing quartzofeldspathic gneiss from the western part of unit II. The S3 mylonitic foliation (S3) is parallel to the S2 foliation. D: Thin D3 mylonite zones (My) and D3 pseudotachylyte vein (Ps) in garnet-bearing quartzofeldspathic gneiss from the northern part of unit V. The mylonite zones, S3 mylonitic foliation (S3) and two pseudotachylyte-generating zones are parallel to S2 foliation (S2) of the surrounding gneiss. E: B5 fold of layered gneiss with remarkable S5 axial foliation (S5) at the western end of unit IV. The S5 foliation is defined by preferred dimensional orientation of elongated coarse orthopyroxene and clinopyroxene grains (Px). F: D6 mylonite zone (D6myz) accompanied by drag fold (synform) (B6) and a metamorphosed and mylonitized mafic dyke (Mmm dyke) along the western part of the boundary fault between units II and III. The D6 mylonite zone is approximately 60 meters in maximum thickness.

Antarctic Geological Map Series

Sheet 1	East Ongul Island 1:5,000	March 1974
Sheet 2	West Ongul Island 1:5,000	March 1974
Sheet 3	Teöya 1:5,000	March 1975
Sheet 4	Ongulkalven Island 1:5,000	March 1975
Sheet 5	Langhovde 1:25,000	March 1976
Sheet 6 & 7	Skarvsnes 1:25,000	March 1977
Sheet 8	Kjuka and Telen 1:25,000	March 1979
Sheet 9	Skallen 1:25,000	March 1976
Sheet 10	Padda Island 1:25,000	March 1977
Sheet 11	Cape Hinode 1:25,000	March 1978
Sheet 12	Lützow-Holm Bay 1:250,000	March 1989
Sheet 13	Prince Olav Coast 1:250,000	March 1989
Sheet 14	Sinnan Rocks 1:25,000	March 1983
Sheet 15	Cape Ryûgû 1:25,000	March 1980
Sheet 16	Akebono Rock 1:25,000	March 1986
Sheet 17	Niban Rock 1:25,000	March 1983
Sheet 18	Kasumi Rock 1:25,000	March 1984
Sheet 19	Tenmondai Rock 1:25,000	March 1985
Sheet 20	Akarui Point and Naga-iwa Rock 1:25,000	March 1984
Sheet 21	Cape Omega 1:25,000	March 1979
Sheet 22	Oku-iwa Rock 1:25,000	March 1981
Sheet 23	Honnör Oku-iwa Rock 1:25,000	March 1987
Sheet 24	Rundvågskollane and Rundvågshetta 1:25,000	March 1986
Sheet 25	Botnneset 1:25,000	March 1987
Sheet 26	Strandnibba 1:25,000	March 1985
Sheet 27 (1)	Mt. Fukushima, Northern Yamato Mountains 1:25,000	March 1978
Sheet 27 (2)	Mt. Torimai, Northern Yamato Mountains 1:25,000	March 1995
Sheet 28	Central Yamato Mountains, Massif B and Massif C 1:25,000	March 1982
Sheet 29	Belgica Mountains 1:25,000	March 1981
Sheet 30	Southern Yamato Mountains (Massif A and JARE-IV) 1:25,000	March 1988
Sheet 31	Balchenfjella 1:100,000	March 1991
Sheet 32	Widerøefjellet 1:100,000	March 1992
Sheet 33	Bergersenfjella 1:100,000	March 1993
Sheet 34	Brattnipene 1:100,000	March 1996
Sheet 35	Sør Rondane Mountains 1:250,000	March 1997
Sheet 36	Ongul Islands 1:10,000	March 1994
Sheet 37	Mount Riiser-Larsen 1:12,500	March 2000
Sheet 38	Tonagh Island 1:10,000	March 2001

GEOLOGICAL MAP OF TONAGH ISLAND
トナー島地質図

Topographic map is plotted by K. Moriwaki, National Institute of Polar Research.
地形図作成は森脇喜一（国立極地研究所）

ANTARCTIC GEOLOGICAL MAP SERIES, SHEET 38 (2001)

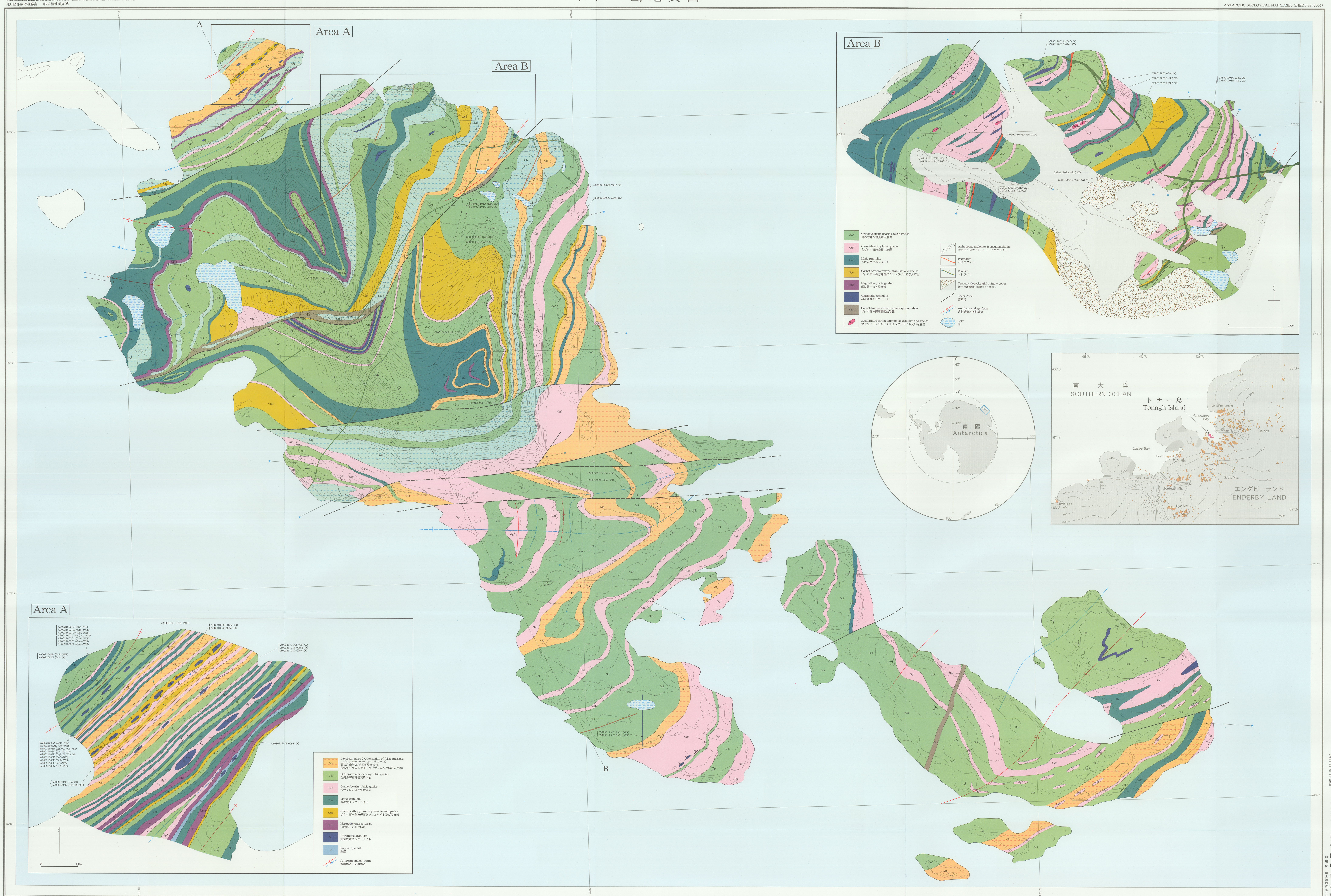

LEGEND 凡例

Paleozoic 古生代
- P — Pegmatite ペグマタイト
- L — Lamproite ランプロアイト

Proterozoic 原生代
- D — Dolerite ドレライト

Archaean 太古代
- Gl1 — Layered gneiss 1 (Alternation of orthopyroxene-bearing felsic gneiss and mafic granulite) 層状片麻岩 1（含斜方輝石珪長質片麻岩及び苦鉄質グラニュライトの互層）
- Gl2 — Layered gneiss 2 (Alternation of felsic gneisses, mafic granulite and garnet gneiss) 層状片麻岩 2（珪長質片麻岩類，苦鉄質グラニュライト及びザクロ石片麻岩の互層）
- Gof — Orthopyroxene-bearing felsic gneiss 含斜方輝石珪長質片麻岩
- Ggf — Garnet-bearing felsic gneiss 含ザクロ石珪長質片麻岩
- Gm — Mafic granulite 苦鉄質グラニュライト
- Ggo — Garnet-orthopyroxene granulite and gneiss ザクロ石ー斜方輝石グラニュライト及び片麻岩
- Gmq — Magnetite-quartz gneiss 磁鉄鉱ー石英片麻岩
- Gu — Ultramafic granulite 超苦鉄質グラニュライト
- Dm — Garnet-two pyroxene metamorphosed dyke ザクロ石ー両輝石変成岩脈

Strike and dip of foliation 面構造の走向傾斜

Shear zone 剪断帯

Antiform and synform 背斜構造と向斜構造

Reclined fold 傾斜褶曲

Rock outcrops where geology is unknown 地質未詳の露岩

A98021801 〈Gsa〉 (MIS) Point and sample number of analyzed rock (X : XRF whole rock chemical analysis, WIS : Sm−Nd whole rock isochron dating, MIS : Sm−Nd mineral isochron dating, IM : U−Pb ion microprobe (SHRIMP) dating, MIR : Rb−Sr mineral isochron dating)
分析試料の採取地点（X : XRF 全岩化学分析，WIS : Sm−Nd 全岩年代，MIS : Sm−Nd 鉱物年代，IM : U−Pb イオンマイクロプローブ (SHRIMP) 年代，MIR : Rb−Sr 鉱物年代）

Locality of sapphirine サフィリンの分布

Mountain peak 山頂

Lake 湖

Sea 海

1 : 10,000

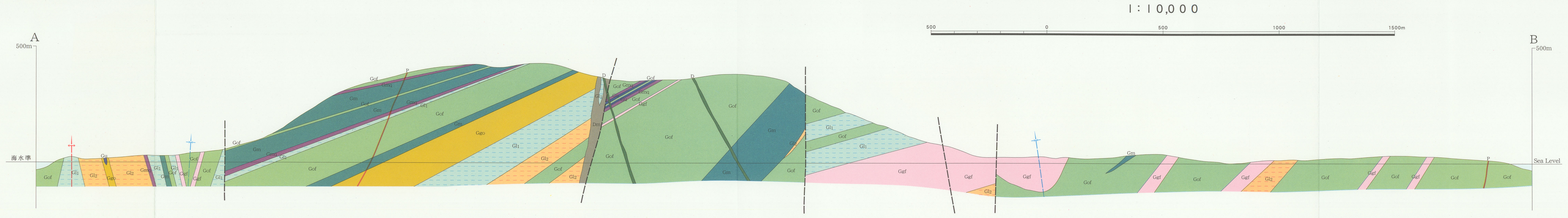

発行責任者 ： 国立極地研究所

地質調査 ： 小山内康人, 豊島剛志, 大和田正明, 角替敏昭, 外田智千, W.A. Crowe 1998 (JARE-39)
本吉洋一, 吉村康隆, 宮本知治, E.S. Grew, C.J. Carson, D.J. Dunkley 1998-1999 (JARE-40)

編集者 ： 小山内康人, 豊島剛志, 大和田正明, 角替敏昭, 外田智千, 吉村康隆, 宮本知治, 本吉洋一

南島部の島々の地質はHarley (1987) による.

国立極地研究所
印刷所 国土地図株式会社

NATIONAL INSTITUTE OF POLAR RESEARCH, TOKYO, JAPAN

Geological survey by Yasuhito OSANAI, Tsuyoshi TOYOSHIMA, Masaaki OWADA, Toshiaki TSUNOGAE, Tomokazu HOKADA and Warwick A. CROWE in 1998 (JARE-39)
Yoichi MOTOYOSHI, Yasutaka YOSHIMURA, Tomoharu MIYAMOTO, Edward S. GREW, Christopher J. CARSON and Daniel J. DUNKLEY in 1998-1999 (JARE-40)

Compiled by Yasuhito OSANAI, Tsuyoshi TOYOSHIMA, Masaaki OWADA, Toshiaki TSUNOGAE, Tomokazu HOKADA, Yasutaka YOSHIMURA, Tomoharu MIYAMOTO and Yoichi MOTOYOSHI

Geology of Southeastern islands is after Harley (1987).

2001
TONAGH ISLAND
トナー島
1 : 10,000